Published for SISSA by Springer

Received: June 2, 2022
Revised: December 28, 2022
Accepted: January 22, 2023
Published: February 9, 2023

Boosted displaced decay of right-handed neutrinos at CMS, ATLAS and MATHUSLA

Priyotosh Bandyopadhyay,[a] **Eung Jin Chun**[b] **and Chandrima Sen**[a]

[a] *Indian Institute of Technology Hyderabad, Kandi, Sangareddy-502285, Telengana, India*
[b] *Korea Institute for Advanced Study, Seoul 02455, Korea*

E-mail: bpriyo@phy.iith.ac.in, ejchun@kias.re.kr, PH19RESCH11014@iith.ac.in

Abstract: We investigate boosted displaced signatures in the Type-I seesaw mechanism associated with the $B-L$ gauge symmetry. Such events arise from decays of right-handed neutrinos depending on their Yukawa couplings and masses. Considering two scenarios: (a) three degenerate right-handed neutrinos whose Yukawa couplings are reconstructed from the observed neutrino masses and mixing; (b) only one right-handed neutrino which decouples from the observed neutrino mass generation and thus its coupling can be arbitrarily small, a detailed PYTHIA based simulation is performed to determine the parameter regions of the $B-L$ gauge boson mass, the neutrino Yukawa couplings, and the right-handed neutrino mass sensitive to CMS, ATLAS, proposed FCC-hh detector and MATHUSLA at the centre of mass energies of 14, 27 and 100 TeV via displaced signatures. We also show in detail how the boost effect enhances the displaced decay lengths, especially for the longitudinal ones, and hinders the probe of Majorana nature of neutrinos.

Keywords: New Gauge Interactions, Other Weak Scale BSM Models, Specific BSM Phenomenology

ArXiv ePrint: 2205.12511

https://doi.org/10.1007/JHEP02(2023)103

JHEP02(2023)103

Contents

JHEP02(2023)103

1 Introduction

The discovery of Higgs boson has proved the correctness of the Standard Model (SM) [1, 2]. Its standard decay modes have been discovered mostly at 5σ-level at both CMS and ATLAS detectors reconstructing the events of di-photon [3, 4], $W^{\pm}W^{\mp}$ [5, 6], ZZ [7, 8], $b\bar{b}$ [9, 10] and $\tau\bar{\tau}$ [11, 12]. Although no phenomenon beyond SM has been observed so far, concerns of various issues viz. light neutrino mass lead us to the extension of SM which still allows the presence of some non-standard exotic decay modes and extra new particles in a vast mass range.

In this article, we consider a simple extension of SM with the gauge group of $\mathrm{U}(1)_{B-L}$. This requires an additional $B-L$ scalar [13–15], and three right-handed neutrinos (RHNs) which are charged under $\mathrm{U}(1)_{B-L}$ and generate small neutrino masses via Type-I seesaw mechanism [16–27]. The $B-L$ scalar is responsible for spontaneous breaking of $\mathrm{U}(1)_{B-L}$ and generating Majorana masses of the right-handed neutrinos. It is also popular to introduce additional scalar as a dark matter candidate which is charged under $\mathrm{U}(1)_{B-L}$ [28–30].

Focusing on relatively light RHNs or very small neutrino Yukawa couplings, we investigate displaced leptonic jet signatures. The RHNs, pair-produced from a heavy $B-L$ gauge boson decay, will have a large boost and rather slow decays into lepton plus jets via (off-shell) W, Z and Higgs bosons. As a consequence, there appear displaced vertices producing boosted collimated lepton plus jets [31], which are almost background free and would be a sensitive probe of the scenario. Such a Fatjet like signature can be easily reconstructed to decrypt the RHN mass. These signatures may come as well with lepton flavor violation and same-sign di-leptons manifesting the Majorana nature of neutrinos. Combining all of these features we will show the future sensitivity of the model parameter space at HL-LHC [32], HE-LHC [33] and FCC-hh [34] with the centre of mass energies of 14, 27 and 100 TeV, respectively. We will also discuss how the boost effect makes it difficult to probe the Majorana nature of neutrinos. In particular the investigations are done with three generations of RHN considering $U_{\rm PMNS}$ and one generation RHNs with the possibility of the displaced leptons that are detectable within MATHUSLA along with CMS, ATLAS and the proposed FCC-hh detector (for 100 TeV centre of mass energy). Though same sign and opposite sign di-leptons coming from RHNs carry the Majorana signature, it can only be probed at the CMS, ATLAS and FCC-hh reference detector. MATHUSLA fails to measure such ratio owing to be situated in one side of the hemispheres of the beam pipe line.

The paper is organized as follows. First we briefly describe main features of the model in section 2. We present the results of our study considering two simple scenarios of Type-I seesaw mechanism: three degenerate right-handed neutrinos in section 3; and only one RHN decoupled from the observed neutrino mass generation in section 4. For each scenario, a `PYTHIA8` based simulation is done with the kinematical distributions to explore displaced vertex signatures at CMS, ATLAS, proposed FCC-hh reference detector and MATHUSLA. We show how the boost effect can skew the Majorana nature of RHNs and how to reinstate it in section 5 and section 6, respectively. Finally we conclude in section 7 with discussion.

2 Model

We extend the Standard Model (SM) with an extra gauge group of U(1) in the minimal $B-L$ framework where the mixing between $\mathrm{U}(1)_Y$ and $\mathrm{U}(1)_{B-L}$ groups are neglected. Thus the Lagrangian obeys the gauge group $\mathrm{SU}(3)_c \times \mathrm{SU}(2)_L \times \mathrm{U}(1)_Y \times \mathrm{U}(1)_{B-L}$. The three generations of right-handed neutrinos are introduced to generate the light neutrino mass via Type-I seesaw mechanism [35, 36]. Here the right-handed neutrinos are though SM gauge singlets but charged under $\mathrm{U}(1)_{B-L}$. However, the $B-L$ symmetry is broken at relatively higher scale when the $B-L$ scalar χ gets vacuum expectation value (vev) and spontaneously generates the Majorana mass (M_N)term for the right-handed neutrinos (N) as well as the $B-L$ gauge boson Z_{B-L}. The charge assignments for the fields are given in table 1 such that $B-L$ anomaly cancels and the theory becomes anomaly free.

The scalar part of the Lagrangian is given by

$$\mathcal{L}_S = (D^\mu \Phi)^\dagger (D_\mu \Phi) + (D^\mu \chi)^\dagger (D_\mu \chi) - V(\Phi, \chi), \tag{2.1}$$

JHEP02(2023)103

	$\mathrm{SU}(3)_c \times \mathrm{SU}(2)_L \times \mathrm{U}(1)_Y$	Y_{B-L}
Φ	(1, 2, 1)	0
N	(1, 1, 0)	-1
L	(1, 2, -1)	-1
Q	(3, 2, 1/3)	1/3
u_R	(3, 1, 4/3)	1/3
d_R	(3, 1, $-2/3$)	1/3
e_R	(1, 1, -2)	1
χ	(1, 1, 0)	2

Table 1. Particle content and there corresponding charges.

with the covariant derivative D_μ can be written as

$$D_\mu = \partial_\mu + ig_2\, T^a\, W^a_\mu + ig_1 Y B_\mu + ig_{BL}\, Y_{B-L}\, B'_\mu. \tag{2.2}$$

Here we use B'_μ for the $\mathrm{U}(1)_{B-L}$ gauge field with strength g_{BL} and hypercharge Y_{B-L}. The total scalar potential in this case can be written as in eq. (2.1),

$$V(\Phi,\chi) = m^2_\Phi \left(\Phi^\dagger\Phi\right) + m^2_\chi|\chi|^2 + \lambda_1\left(\Phi^\dagger\Phi\right)^2 + \lambda_2|\chi|^4 + \lambda_3\Phi^\dagger\Phi|\chi|^2, \tag{2.3}$$

where Φ is the complex scalar SM Higgs doublet, $\Phi = \left(\phi^\dagger\ \phi^0\right)^T$ and χ is the complex $B-L$ scalar which is singlet under SM gauge group. The $B-L$ gauge group is broken spontaneously when χ attains a vev, v_{BL} i.e. at the $B-L$ breaking we can write $\chi = (v_{BL} + \chi_0 + i\chi')/\sqrt{2}$. Similarly, the SM gauge group is also broken when ϕ^0 gets a vev, i.e. at $\phi^0 = (v+h)/\sqrt{2}$ and we are left with only electromagnetic and SU(3) as symmetric gauge group. After symmetry breaking we have two mass eigenstates $h_{1,2}$, where $h_1 \sim h_{\rm SM}$ satisfying the Higgs data [1, 2].

As can be read from eq. (2.4), the RHNs couple to SM Higgs doublet via $Y_{N_{ij}}$ and with $B-L$ scalar via $\lambda_{N_{ij}}$ Yukawa terms respectively, where i, j are generation indices.

$$\begin{aligned}\mathcal{L}_Y \;=\; & -Y^u_{ij}\,\overline{Q}_i\,\tilde{\Phi}(u_R)_j - Y^d_{ij}\,\overline{Q}_i\,\Phi(d_R)_j - Y^e_{ij}\,\overline{L}_i\,\Phi(e_R)_j \\ & - \underbrace{(Y_N)_{ij}\,\overline{L}_i\,\tilde{\Phi}N_j}_{\text{Dirac mass term}} - \underbrace{(\lambda_N)_{ij}\,\chi\overline{N}^C_i\,N_j}_{\text{Majorana mass term}},\end{aligned} \tag{2.4}$$

where, $\tilde{\Phi} = i\sigma^2\Phi^*$ and i, j denote three fermion generations. Here the $B-L$ breaking vev i.e. v_{BL} generates the Majorana neutrino mass term for the RHNs as $M_N = 2\lambda_N\langle\chi\rangle$ and the Dirac mass term is generated via the vev of EWSB i.e. v as $m_D = \frac{Y_N v}{\sqrt{2}}$. The $B-L$ gauge boson also becomes massive by absorbing the Goldstone boson corresponding to the $B-L$ symmetry, which is given as $M_{Z_{B-L}} = 2g_{BL}v_{BL}$. Thereafter, the three light neutrinos can be generated through the Type-I seesaw mechanism [35] by diagonalizing

JHEP02(2023)103

eq. (2.5), which gives rise to the mass eigenvalues as shown in eq. (2.6)

$$\mathcal{M}_\nu = \begin{pmatrix} 0 & m_D \\ m_D^T & M_N \end{pmatrix}, \tag{2.5}$$

where the obtained masses of light and heavy neutrinos are,

$$M_{\nu_L} \simeq \frac{Y_N^2\, v^2}{2M_N} \quad \text{and,} \quad M_{\nu_R} \simeq M_N. \tag{2.6}$$

Here for simplicity we have dropped the generation indices.

3 Scenario-1

Here we consider the three generations of RHNs considering the light neutrino masses and mixing data as described below. The case of only one of the RHNs with light Yukawa is discussed in section 4.

3.1 Parameter space and benchmark points

We consider first the Type-I seesaw mechanism with three degenerate RHNs where $N_{1,2,3}$ have same mass M_N. Adopting the Casas-Ibarra parameterization [37], one can reconstruct their Yukawa matrix given the active neutrino mass matrix compatible with the observations. Taking the central values of the neutrino oscillation parameters with the normal ordering [38], we get the following neutrino mass matrix:

$$M_\nu \approx \begin{pmatrix} 0.0030 - 0.0008i & 0.0001 + 0.0052i & -0.0043 + 0.0047i \\ 0.0001 + 0.0052i & 0.030 + 0.00045i & 0.021 \\ -0.0043 + 0.0047i & 0.021 & 0.025 \end{pmatrix} \text{eV}$$

This can be reproduced by the following Yukawa matrix.

$$Y_N = \begin{pmatrix} 0.62 - 0.33i & -0.54 + 0.30i & -0.77 - 0.30i \\ -2.01 + 0.046i & 0.83 - 0.039i & -2.23 - 0.09i \\ -1.41 + 0.042i & 2.34 - 0.036i & -0.93 - 0.083i \end{pmatrix} \times 10^{-7} \sqrt{\frac{M_N}{100\text{GeV}}} \tag{3.1}$$

One can see that $\sum_{\alpha=e,\mu,\tau} |Y_{N,\alpha k}|^2 = 6.54 \times 10^{-14}\, M_N/100\text{GeV}$ for each N_k ($k = 1, 2, 3$, the indices for three generations of RHN). Thus, generation wise the branching ratio matrix is given by

$$\text{BR}_{\alpha k} = \begin{pmatrix} 0.0758772 & 0.0577112 & 0.104687 \\ 0.618174 & 0.105466 & 0.762472 \\ 0.305949 & 0.836823 & 0.132842 \end{pmatrix} \times B(N \to XY)_{\text{diag}}, \tag{3.2}$$

where $B(N \to XY)_{\text{diag}}$ is the decay branching fraction of the RHN in a particular mode for the choice of diagonal Yukawa couplings. For example for diagonal choice of the Yukawa

JHEP02(2023)103

Benchmark points	BP1	BP2	BP3
M_N in GeV	10	60	100
$M_{Z_{BL}}$ in TeV	5.0	5.0	5.0

Table 2. Choice of benchmark points in terms of RHN and Z_{B-L} mass for the collider study.

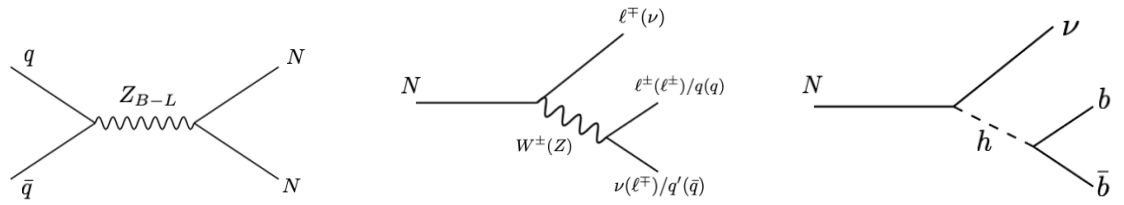

Figure 1. Feynman diagrams for generating RHN pairs via Z_{B-L} at the LHC (a) and their further decays (b, c).

Y_N, and $M_N = 500\,\text{GeV}$, the N_k decays to $W^{\pm}\ell_k^{\mp}$, $Z\nu_{\ell_k}$, $h\nu_{\ell_k}$ in 2:1:1 ratio. For a given choice of generic Yukawa coupling including off-diagonal entries like eq. (3.1), the generation splitting of a particular decay modes can be found from eq. (3.2). One can estimate the total contribution for a given decay modes from the three generations of RHN by summing over the RHN generations, for each generation of SM leptons as $\sum_k \text{BR}_{\alpha k} = (0.238, 1.486, 1.276) \times B(N \to XY)_{\text{diag}}$. The average decay branching fraction for a given mode can be obtained as $\frac{1}{3}\sum_k \text{BR}_{\alpha k}$.

For the study of this scenario, we set up the three benchmark points in table 2. The heavy Higgs boson which is also charged under $\text{U}(1)_{B-L}$ can in principle give rise to RHN pair or $N\nu$ via the two-body decays [36, 39, 40], which are taken to be negligible in our study. Essential bounds on this model come from the searches of Z_{B-L} via di-leptonic resonance at LEP and LHC that put strong bound on $M_{Z_{B-L}}$, g_{BL}. Z_{B-L} is searched via $e^{\pm}e^{\mp}$ and $\mu^{\pm}\mu^{\mp}$ modes at the LEP [41, 42] and a strong bound was put as $M_{Z_{B-L}}/g_{BL} = Y^{\chi}_{B-L}v_{BL} > 6\,\text{TeV}$ [41, 42]. Similarly, the most recent data of ATLAS [43] and CMS [44] LHC at 13 TeV have put new constraints on cross-section$\times$ branching fractions in the di-lepton final states till $M_{Z_{B-L}} = 6\,\text{TeV}$. However, such bound can be relaxed in our case due to the reduced decay branching fraction of Z_{B-L} to di-lepton, owing to the additional decay modes to heavy neutrinos.

In our case the right-handed neutrino is charged under $B - L$, which opens up the possibility of Z_{B-L} decays to N pairs. We see from figure 1(a) that the Z_{B-L} can produce RHN pair, similar to the di-leptonic pair, which further can decay into $W^{\pm}l^{\mp}$ and $Z\nu$ as shown in figure 1(b) if RHN is heavier than the $W^{\pm}, Z$ mass viz., BP3, where RHN mass is 100 GeV. For RHN mass greater than SM Higgs mass the $N \to h\nu$ mode is open as shown in figure 1(c). The partial decay width for the RHN into on-shell $W^{\pm}$, Z, h are given by

JHEP02(2023)103

eq. (3.3)–(3.5).

$$\Gamma(N \to W^+ l^-) = \Gamma(N \to W^- l^+) = \frac{Y_N^2 M_N}{32\pi}\left(1 - \frac{M_W^2}{M_N^2}\right)^2\left(1 + \frac{2M_W^2}{M_N^2}\right), \tag{3.3}$$

$$\Gamma(N \to Z\,\nu) = \Gamma(N \to Z\,\bar{\nu}) = \frac{Y_N^2 M_N}{64\pi}\left(1 - \frac{M_Z^2}{M_N^2}\right)^2\left(1 + \frac{2M_Z^2}{M_N^2}\right), \tag{3.4}$$

$$\Gamma(N \to \nu\, h) = \Gamma(N \to \bar{\nu}\, h) = \frac{Y_N^2 M_N}{64\pi}\left(1 - \frac{M_h^2}{M_N^2}\right)^2. \tag{3.5}$$

However, for BP1 and BP2 the RHN masses are 10 GeV and 60 GeV respectively, for which $W^\pm$, Z both are off-shell, leading to three-body decays of RHN to light quarks and leptons. The partial three-body decay rates are in this case proportional to the mixing i.e. Y_N^2 [45] as given in eq. (3.6)–(3.10). The the corresponding decay branching fractions are incorporated during the simulation appropriately.

$$\Gamma(N \to \ell_1^- \ell_2^+ \nu) = \Gamma(N \to \ell_1^- \ell_2^+ \nu) = |Y_N|^2 \frac{G_F^2 M_N^5}{192\pi^3}, \tag{3.6}$$

$$\Gamma(N \to \ell^- q_1 \bar{q}_2) = \Gamma(N \to \ell^+ \bar{q}_1 q_2) = |Y_N|^2 \frac{G_F^2 M_N^5}{192\pi^3}\, N_C\, |K_{q_1 q_2}|^2, \tag{3.7}$$

$$\Gamma(N \to \nu \bar{\ell}' \ell') = \Gamma(N \to \bar{\nu} \ell' \bar{\ell}') = |Y_N|^2 \frac{G_F^2 M_N^5}{192\pi^3}(C_L^2 + C_R^2), \tag{3.8}$$

$$\Gamma(N \to \nu q \bar{q}) = \Gamma(N \to \bar{\nu} \bar{q} q) = |Y_N|^2 \frac{G_F^2 M_N^5}{192\pi^3}\, N_C \left[(C_L^q)^2 + (C_R^q)^2\right], \tag{3.9}$$

$$\Gamma(N \to \nu_\ell \nu_{\ell'} \bar{\nu_{\ell'}} = \Gamma(N \to \bar{\nu_\ell} \nu_{l'} \bar{\nu_{\ell'}}) = |Y_N|^2 \frac{G_F^2 M_N^5}{192\pi^3}\, C_\nu^2, \tag{3.10}$$

where $N_C = 3$, number of color degrees of freedom of quark and K_{q_1,q_2} is the CKM matrix element. The various couplings in terms of C are given by

$$C_L = -\frac{1}{2} + \sin^2\theta_W, \qquad C_R = \sin^2\theta_W, \qquad C_\nu = \frac{1}{2}, \tag{3.11}$$

$$C_L^u = \frac{1}{2} - \frac{2}{3}\sin^2\theta_W, \qquad C_R^u = -\frac{2}{3}\sin^2\theta_W, \tag{3.12}$$

$$C_L^d = -\frac{1}{2} + \frac{1}{3}\sin^2\theta_W, \qquad C_R^d = \frac{1}{3}\sin^2\theta_W. \tag{3.13}$$

We calculate the $\sigma \times \mathcal{B}(Z_{B-L} \to \ell^+\ell^-)$ for the benchmark points mentioned in table 2 for 13 TeV centre of mass energy and presented them against the 13 TeV bounds from ATLAS [43] in figure 2 and it can be seen that our chosen point is allowed by the ATLAS bound. In this figure the black dashed and purple dot-dashed lines are for expected limits on the cross-section, at the relative width-signals of zero and 10%, respectively [43]. The green line is for the $\mathrm{U}(1)_{B-L}$ Model, where the gauge couplings are taken as $g_{BL} = 0.3$. It can be seen that the chosen benchmark point is allowed by both the LEP data [46] and collider limits from LHC [43, 44].

The chosen benchmark points are further looked into for different final state topologies at the LHC with centre of mass energies of 14 TeV, 27 TeV and 100 TeV, respectively. Once

JHEP02(2023)103

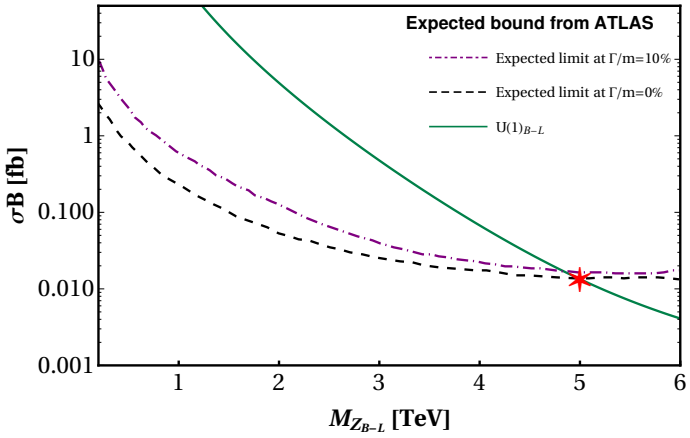

Figure 2. Constraints from σB coming from di-leptonic final state at the LHC with the centre of mass energy of 13 TeV and luminosity of 139 fb^{-1} [43]. The black dashed and purple dot-dashed lines are for expected limits on the cross-section, at the relative width-signals of zero and 10%, respectively. The green line represents the theoretical prediction of $\text{U}(1)_{B-L}$ model. The red star is the chosen benchmark point for the collider study.

Benchmark points	Centre of mass energy		
	14 TeV	27 TeV	100 TeV
BP1	0.083	1.63	45.75
BP2	0.077	1.61	45.66
BP3	0.073	1.60	45.51

Table 3. Drell-Yan cross-section in fb for $pp \to NN$ for the three generations at LHC. We calculate it with three different center of mass energies, 14 TeV, 27 TeV and 100 TeV for chosen benchmark points.

the RHNs are produced via Z_{B-L} they would decay to $\ell^{\mp}W^{(*)\pm}$, $\nu Z^{(*)}$, or $\nu h^{(*)}$ as shown in figure 1 (b) and (c). The on-shell gauge bosons can further decay hadronically or they can produce leptons and missing energy. Since we choose BP1 and BP2 for comparatively low mass of RHN, the intermediate gauge bosons are off-shell. We can see the evidences of off-shell decay in the subsequent sections as the RHN mass is very small around 10 GeV, it decays to $W^{*\pm}\ell^{\mp}$ and can produce displaced di-leptons and a neutrino. In this case due to extra boost coming from RHNs, the leptons will be very co-linear and form almost a `di-leptonic jet` structure.

Contrary to the only Type-I seesaw mechanism, where the pair production of RHN solely depends on the mixing angle $\theta^2 \sim (\frac{Y_N v}{\sqrt{2}M_N})^2$, here it can be mediated via the Z_{B-L} gauge boson enhancing the production cross-section. The production cross-section for three benchmark points with three different centre of mass energies i.e., 14 TeV, 27 TeV and 100 TeV, respectively at the LHC /FCC are shown in table 3. We generate the model files in `SARAH` [47] and they are fed to `CalcHEP` [48], which is used to calculate the cross-section with the `NNPDF23_LO` as parton distribution function [49] using the renormalization/factorization

JHEP02(2023)103

scale of $\sqrt{\hat{s}}$, where s is the partonic level centre of mass energy of the interaction. We can see that the production cross-section is a bit low at the LHC for 14 TeV centre of mass energy because of the high mass of Z_{B-L}. As we increase the RHN mass from BP1 to BP3 keeping the Z_{B-L} mass fixed, the cross-section changes infinitesimally, which is not very significant from the collider perspective. It can be noticed that for 100 TeV centre of mass energy the cross-section is enhanced to 45 fb.

3.2 Collider simulation and kinematical distributions

In this section, we perform the collider simulation at the HL-LHC/HE-LHC/FCC for three different centre of mass energies i.e. 14, 27 and 100 TeV, respectively for the chosen benchmark points and also discuss their displaced vertex signatures at the CMS, ATLAS, proposed FCC-hh reference detector [34, 50, 51] and MATHUSLA [52] in the next sections. For BP1 and BP2 the RHNs decay via three-body decays. On the contrary for BP3, the RHNs decay via two-body decays. We will explore how the boost effect influences the final state topologies of these two distinct types of scenarios. For our study the RHN mass is less than the SM Higgs boson mass for all BPs and thus it cannot be produced on-shell. However, during the sensitivity reach plots in subsection 3.6 and subsection 4.4, the appropriate decay branching fractions are taken into account.

For the collider simulation we generate the events (.lhe files) via `CalcHEP` and simulate those via `PYTHIA8` [53] with initial state and final state radiations. Hadronization and its decays are also done by `PYTHIA8`, whereas for the jet formation we use `Fastjet-3.0.3` [54] with the `ANTI-KT` algorithm with the jet cone size $R = 0.5$. Initial state radiation (ISR) and final state radiation (FSR) are switched on during the collider simulation. The other basic cuts are as follows:

- The pseudorapidity for the calorimeter coverage is $|\eta| < 4.5\,(6)$ for 14, 27 (100) TeV colliders.
- The minimum transverse momentum for jets is $p_{T,\text{min}}^{\text{jet}} = 20\,(25)$ GeV for 14, 27 (100) TeV colliders.
- We choose the leptons with $p_T > 10\,(3)$ GeV and $|\eta_{\text{max}}| = 3.8\,(4.8)$ for 14, 27 (100) TeV colliders.
- For a selection of clean leptons, we put a cut on the total transverse momentum of the hadrons within the cone $\Delta R = 0.3$, demanding it to be $\leq 0.15\ p_T^l$. Here p_T^l is the transverse momentum for the leptons within that specified cone.
- Additionally, the leptons are isolated from the clustered jets with $\Delta R_{lj} \geq 0.1$.

The isolated charged leptons ($e^{\pm}$ and $\mu^{\pm}$) are tagged as the final state leptons. Those can come directly from the right-handed neutrinos or from the decay of intermediate gauge bosons $W^{\pm}$, Z. Below we describe the kinematical distributions at the LHC only with centre of mass energy of 14 TeV for the benchmark points. Here the kinematical distributions show the normalised event numbers for a given integrated luminosity as $n^{\text{obs}} = \frac{1}{N} \times n^{\text{sim}} \times \sigma \times \int \mathcal{L} dt$.

JHEP02(2023)103

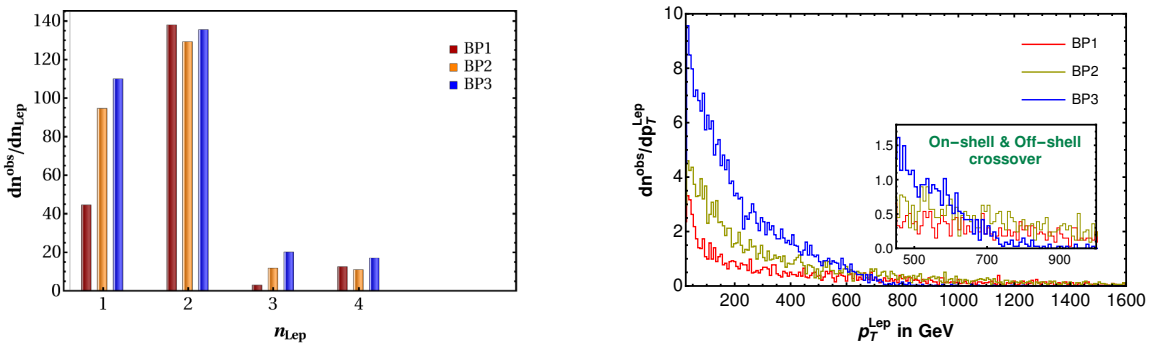

(a) (b)

Figure 3. The lepton $(e^{\pm}, \mu^{\pm})$ multiplicity distributions, $n_{\rm Lep}$ (a), and the lepton p_T distributions, $p_T^{\rm Lep}$ for the first lepton only (b), for the benchmark points at the centre of mass energy of 14 TeV with the integrated luminosity of $3\,{\rm ab}^{-1}$.

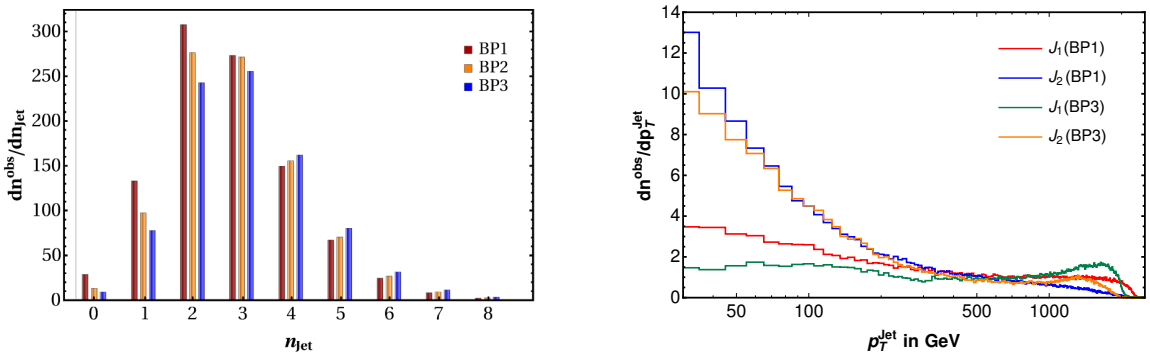

(a) (b)

Figure 4. The Jet multiplicity distribution $(n_{\rm jet})$ for three benchmark points (a), and the p_T distribution $(p_T^{\rm jet})$ of the 1^{st} and 2^{nd} Jets with BP1 and BP3 (b) are shown at the centre of mass energy of 14 TeV with the integrated luminosity of $3\,{\rm ab}^{-1}$.

Figure 3(a) describes the lepton multiplicity distribution for the benchmark points. For the benchmark points the lepton at higher multiplicity are significantly low in numbers due to the low effective branching and also due to the isolation cuts as mentioned above. The multiplicity distributions peak around $n_{Lep} = 2$ for all three cases, as the $W^{\pm}$ bosons mostly decay hadronically. In figure 3(b) we present the transverse momentum distributions of the first lepton i.e., p_T^{ℓ} for the benchmark points. In case of BP3, the RHN (N) has a on-shell decay to either $\ell^{\pm}W^{\mp}$ or $Z\nu$. Thus, the leptons come from the on-shell decays of these gauge bosons have shorter tail in p_T^{ℓ} compared to the ones coming directly from RHNs in case of BP1 and BP2 due to the direct boost effect from the RHN. For BP1 and BP2, the RHNs go through off-shell three-body decays, where we cannot distinguish the two leptons coming from a single RHN leg and thus share the momentum equally leading to a larger tail for the higher momentum as can be seen from the inset of figure 3(b). Thus a cross-over around $p_T^{\ell} \sim 700\,{\rm GeV}$ among BP3 and BP1 or BP2 can be noticed.

JHEP02(2023)103

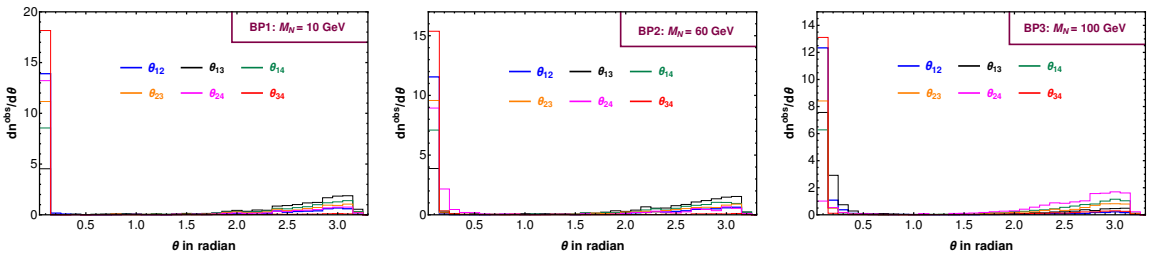

(a) (b) (c)

Figure 5. The angular distribution (θ) of the angles between two leptons at the LHC with the centre of mass energy of 14 TeV and the integrated luminosity of 3 ab^{-1} for the benchmark points.

We depict the jet multiplicity distribution for the benchmark points in figure 4(a). We see that for all three BPs the multiplicity distributions peaks around two or three, which is expected when only one of the gauge boson (either $W^{\pm}$ or Z) decays hadronically along with a ISR/FSR jet or both the gauge bosons decay hadronically but one jet is missed or two jets are merged as one. The maximum partonic jet multiplicity should be around four; however, due to ISR/FSR the jet multiplicity can go up to eight. In figure 4(b) we describe the first and second p_T ordered jets for BP1 and BP3, respectively. A cross over of $p_T^{\rm jet}$ like lepton p_T around 700 GeV is also noticed.

After dealing with the leptons and jet kinematic distributions, we focus on the angles between the leptons (θ_{ij}) which are already isolated from the jets. The leptons coming from the decays of RHNs can be very co-linear with the leptons that is coming from on- or off-shell $W^{\pm}$ of the same RHN leg, due to the boost effect. This can form a scenario where two extremely co-liner charged leptons can come as `leptonic jet`. In figure 5 we show how the opening angles among the leptons are distributed for three different benchmark points. It is evident to see that for θ_{12} (in blue) and θ_{34} (in red) peaks around zero, which points out the fact that ℓ_1, ℓ_2 are coming from same RHN leg and ℓ_3, ℓ_4 are coming from different RHN leg. Thus, the distribution helps us to figure out the correct leg which forms the `leptonic jet`. However, from figure 5(a) one can see that such effects are more prominent for the case $M_N = 10$ GeV (BP1) and the effect gets reduced as we increase the RHN mass as can be seen from figure 5(c) for $M_N = 100$ GeV (BP3).

3.3 Reconstruction of RHN mass

One of the parameters which can lead to the discovery of RHN is the invariant mass distribution. In figure 6, we summarize the invariant mass distributions towards the reconstructions of the $W^{\pm}$ boson for the benchmark points. For BP1 and BP2 the RHN mass is 10, 60 GeV, respectively, which are less than the $W^{\pm}$, making it off-shell. Figure 6(a) depicts the scenario of BP1 ($M_N = 10$ GeV), where the two-jets coming from an off-shell $W^{\pm}$ boson are collimated forming a single jet, known as Fatjet [55–59]. Thus, an invariant mass distribution of $M_{j\ell}$ shows the peak around 10 GeV in figure 6(a), which designates the RHN mass for the BP1. Similar situation can also be realized for BP2, where $M_{j\ell}$ peaks around 60 GeV as can be seen in figure 6(b). In table 4 the reconstructions are

JHEP02(2023)103

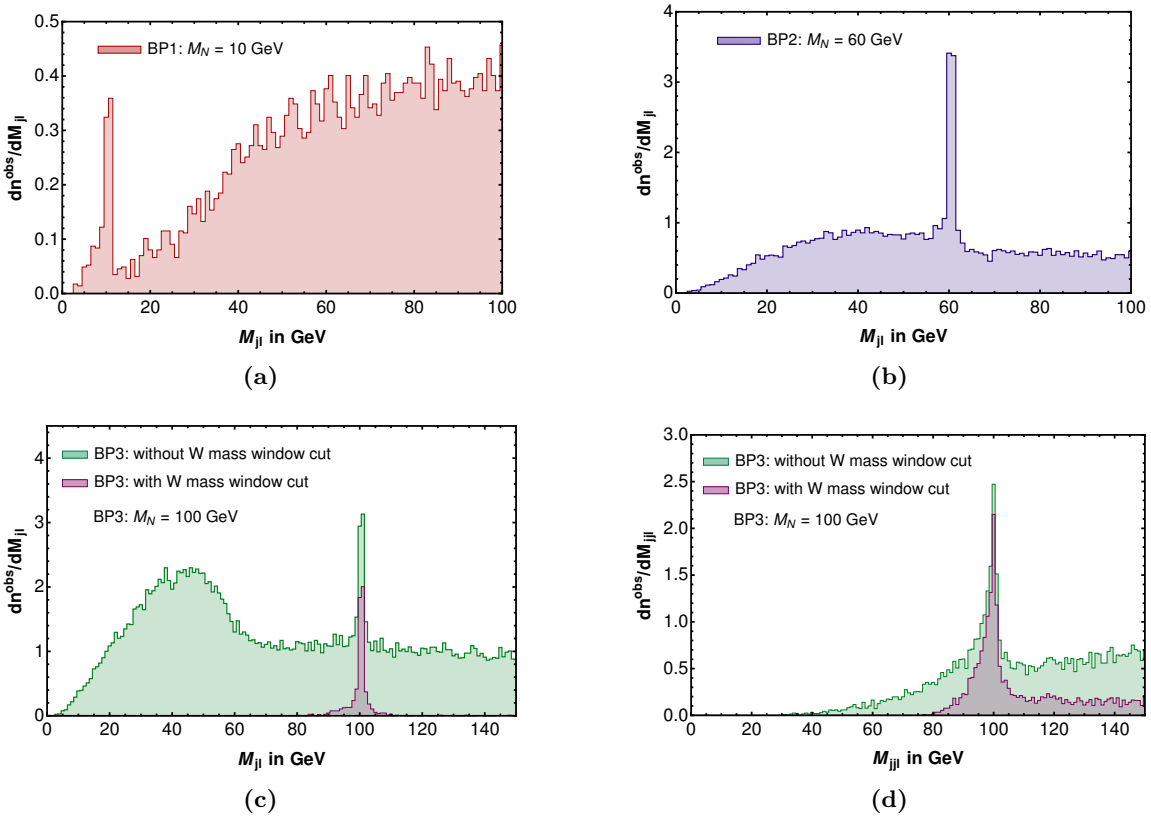

Figure 6. Reconstruction of RHN mass from heavily boosted Fatjet and mono-lepton (M_{jl}) for BP1, BP2, BP3 (a, b, c) and mono-lepton-di-jet invariant mass for BP3 (d) at the LHC with the centre of mass energy of 14 TeV and the integrated luminosity of 3 ab^{-1}. The purple colour represents the distribution after applying a window cut of 10 GeV around $W^{\pm}$ mass, while the green represents the distribution of M_{jl} and M_{jjl} for BP3 in (c) and (d), respectively.

demonstrated via the number of events in $M_{j\ell}$ distributions after the window cut around the mass peak for BP1, BP2 with the centre of mass energies of 14, 27, 100 TeV at the integrated luminosities of ($\mathcal{L}_{\rm int}$ =) 3, 10 and 30 ab^{-1}, respectively considering the goal of the different colliders, HL-LHC, HE-LHC and FCC-hh [51]. For BP2 and with centre of mass energies of 27, 100 TeV look promising.

However, the situation changes a lot, when $W^{\pm}$ is produced on-shell from the RHN decay in the case of BP3. Two quarks coming from the $W^{\pm}$, can be collimated and form a single jet or they can also form two different jets. As the previous case the analysis would be similar and they are presented in figure 6(c). Contrary to the previous two cases (for BP1 and BP2), here a single jet mass can be around the on-shell $W^{\pm}$ mass, and a reconstruction of RHN mass with the jet coming from the $\pm$10 GeV of the $W^{\pm}$ boson mass, is presented by the purple graph. Whereas, the green curve shows such reconstruction without any demand of $W^{\pm}$ mass reconstruction. Though the number of events in the previous case is little lower than the later one, the peak is sharper in the previous case and we consider that for final state number presented latter in the text. The corresponding

JHEP02(2023)103

Benchmark Points	$M_{j\ell}$	Centre of mass energy		
		14 TeV	27 TeV	100 TeV
BP1	$\lvert M_{j\ell} - 10.0\rvert \leq 5\,\text{GeV}$	0.8	13.1	611.3
BP2	$\lvert M_{j\ell} - 60.0\rvert \leq 5\,\text{GeV}$	8.7	388.4	36911.7

Table 4. The number of events in $M_{j\ell}$ distributions after the window cut around the mass peak for BP1, BP2 with the centre of mass energies of 14 TeV, 27 TeV, 100 TeV at the integrated luminosities of ($\mathcal{L}_{\text{int}} =$) 3, 10 and 30 ab^{-1}, respectively.

Benchmark Point	$M_{j\ell}/M_{jj\ell}$	Centre of mass energy		
		14 TeV	27 TeV	100 TeV
BP3	$\lvert M_j - 80.0\rvert \leq 10\,\text{GeV}$ & $\lvert M_{j\ell} - 100.0\rvert \leq 10\,\text{GeV}$	5.0	175.2	16401.7
	$\lvert M_{jj} - 80.0\rvert \leq 10\,\text{GeV}$ & $\lvert M_{jj\ell} - 100.0\rvert \leq 10\,\text{GeV}$	4.5	156.5	10674.3

Table 5. The number of events in $M_{j\ell}$ and $M_{jj\ell}$ distributions after the window cut around the mass peak for BP3 with the centre of mass energies of 14 TeV, 27 TeV, 100 TeV at the integrated luminosities of ($\mathcal{L}_{\text{int}} =$) 3, 10 and 30 ab^{-1}, respectively. An additional window cut of 10 GeV around the $W^{\pm}$ mass peak is also implemented while reconstruction of RHN mass.

events number for $M_{j\ell}$ for $2\ell + 2j$ final state are given in table 5 after the window cut around the mass peak for BP3 with the centre of mass energies of 14 TeV, 27 TeV, 100 TeV at the integrated luminosities of ($\mathcal{L}_{\text{int}} =$) 3, 10 and 30 ab^{-1}, respectively.

The other possibility, where the two quarks are not boosted enough and form two separate jets, can establish $W^{\pm}$ mass peak via M_{jj}, which can be seen in figure 6(d). Following similar approaches of with and without the $W^{\pm}$ mass window cuts, one can reconstruct the RHN mass around 100 GeV, for the BP3. The events corresponding to $M_{jj\ell}$ distributions for $2\ell + 4j$ are given in table 5 after the window cut around the mass peak for BP3 with the centre of mass energies of 14 TeV, 27 TeV, 100 TeV at the integrated luminosities of ($\mathcal{L}_{\text{int}} =$) 3, 10 and 30 ab^{-1}, respectively.

3.4 Displaced vertex signatures

A particle, in this case the RHN, can have displaced decay with rest mass decay length $L_0 = c\tau_0 = \frac{c}{\Gamma_0}$, where Γ_0 is the rest decay width. Generic decays follow the exponential distribution as given below

$$N(\tau) \propto \exp(-\tau/\tau_0), \tag{3.14}$$

where N is number corresponding to the actual decay life time τ, and τ_0 is the rest mass decay time. On top of that, the boost effect can enhance such decay lengths further, i.e.

JHEP02(2023)103

Benchmark points	Decay width (in GeV)	Rest mass decay length (in m)
BP1	1.02×10^{-18}	193.00
BP2	4.97×10^{-17}	3.96
BP3	9.25×10^{-15}	0.02

Table 6. Decay widths and rest mass decay lengths for the benchmark points.

the resultant decay length is given by [60]

$$L_\tau = c\tau\beta\gamma = \tau\frac{p}{m}, \tag{3.15}$$

where p is three momentum of the particle and m is the rest mass. The momentum measured in the transverse and longitudinal directions can lead to displaced decay lengths of $L_\perp$, $L_{||}$ as given by

$$L_\perp = \tau\frac{p_\perp}{m}, \quad L_{||} = \tau\frac{p_{||}}{m}. \tag{3.16}$$

Defining the transverse and longitudinal displaced decay lengths considering the corresponding boosts, we will see that LHC at higher centre of mass energies can lead to more longitudinal boost governed by the parton distribution function than the transverse one, which is mainly dependent on the uncertainty principle. We show $L_\perp$, $L_{||}$ distributions (in figure 9 and in figure 11) separately in order to show the different boost effects for the perpendicular and longitudinal decay lengths. However, for the event number inside the detector of length L, we consider the total decay length of the RHN $L_\tau = \tau\frac{p}{m}$, and the number of events inside the detector is given by $N(L; L_\tau) = N_0(1 - \exp(-L/L_\tau))$, where N_0 is the initial number of particles. Here we pick a conservative minimum value for the boosted decay length of the RHNs of 1 mm [61, 62] is taken into account as displaced.

We consider two scenarios to study the displaced decays of the RHNs. For the three BPs in scenario-1 , the root sum square values of the Yukawa couplings are $Y_N = 8.08 \times 10^{-8}$, 1.98×10^{-7}, and 2.56×10^{-7} for BP1, BP2, and BP3, respectively. The corresponding decay lengths are tabulated in table 6. In scenario-2, we consider BP2 and BP3 only, with the Yukawa couplings $Y_N = 5 \times 10^{-8}$, 5×10^{-9} and the details are discussed in section 4.

The CMS [63] and ATLAS [64] detectors at the LHC can detect displaced decay signatures for the long lived particles up to 7.5 ($L_\perp$), 12.5 ($L_\perp$) meters, and 11 ($L_{||}$), 22 ($L_{||}$) meters, respectively from the interaction point (IP) in the transverse ($L_\perp$) and the longitudinal ($L_{||}$) directions. The corresponding lengths for the proposed detector of FCC-hh [34, 50, 51] is 10 ($L_\perp$) and 25 ($L_{||}$) meters, respectively from the IP. The limitations of detecting displaced vertex signatures with larger decay lengths $\mathcal{O}(100)$ m at the CMS, ATLAS and FCC-hh detector led to the proposal of MATHUSLA [52, 65–68] detector, which will be placed on the LHC beam pipe, 68 m away from the centre of the LHC detectors as depicted in figure 7(a). It should be notated that MATHUSLA detector is planned to be placed in one side of the hemispheres, thus it can only tag maximum one RHN at a time. Thus the same and opposite sign leptons coming from both the legs of RHN remain illusive for MATHUSLA.

JHEP02(2023)103

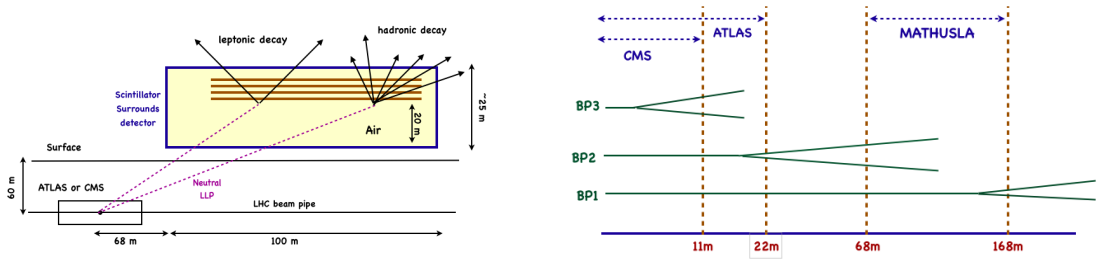

(a) (b)

Figure 7. A schematic diagram for MATHUSLA detector [68] and the rest decay points of chosen BPs.

According to a recent update, the MATHUSLA detector will be 68 meters from the CMS/ATLAS interaction point in the longitudinal direction, 60 meters in the transverse direction and will have a volume of $25 \times 100 \times 100\,\mathrm{m}^3$, with a access over the azimuthal angle of 0.27. The corresponding η cuts are taken care of by demanding the transverse and longitudinal decay lengths within the detectors simultaneously. The detecting efficiency for the hadronic as well as leptonic decays are almost 100% [52, 69]. In figure 7(b) the rest mass decay lengths are exhibited for the benchmark points as mentioned in table 6. As evident from table 6, for BP2 and BP3 the rest mass decay length $\lesssim 10$ m and fall within the range of CMS and ATLAS detector. For the boost effect, we can still get some events in the MATHUSLA region for BP2. However, for BP1, it is ~ 193 m, which falls beyond the MATHUSLA region. It is worth mentioning here that, as the 100 TeV FCC-hh is not built yet, one can take the liberty of suggesting LLP (Long Lived particle) detectors with location and geometry suited to one's model and search strategies for example in [70]. However, the MATHUSLA geometry is better for the LLPs in our consideration even at 100 TeV FCC-hh.

In figure 8 we present the displaced decay length contours of RHN from 0.001 m to 500.0 m in $M_N - Y_N$ plane with different shaded regions. We also mention the boundaries of CMS and ATLAS detectors with magenta solid and dashed lines, respectively with the regions in the right that can be explored. MATHUSLA will be implemented approximately 68 m away from LHC and the region that can be traversed is shown by the light brown band in figure 8. Along with MATHUSLA, FASER-II [71, 72] is also proposed to be placed at a distance of 480 m in the longitudinal direction from ATLAS interaction point. This detector will be only 10 m long and its radius is proposed to be only 1 m. It can detect the events with $|\eta| \geq 3.5$. Thus the main motivation of FASER-II is to detect the soft events coming along with beam pipe line.

Equipped with the collider set up and with the knowledge of the rest mass decay lengths, we plot the transverse ($L_\perp$ in red) and longitudinal ($L_{||}$ in green) decay length distributions for the benchmark points at the LHC/FCC for the centre of mass energies of 14 (a, d, g), 27 (b, e, h), 100 TeV (c, f, i) with the integrated luminosities of 3, 10 and 30 ab^{-1}, respectively in figure 9. The plots are generated by PYTHIA8 [53], where the boost effects and the decay distributions are included dynamically event by event. The CMS

JHEP02(2023)103

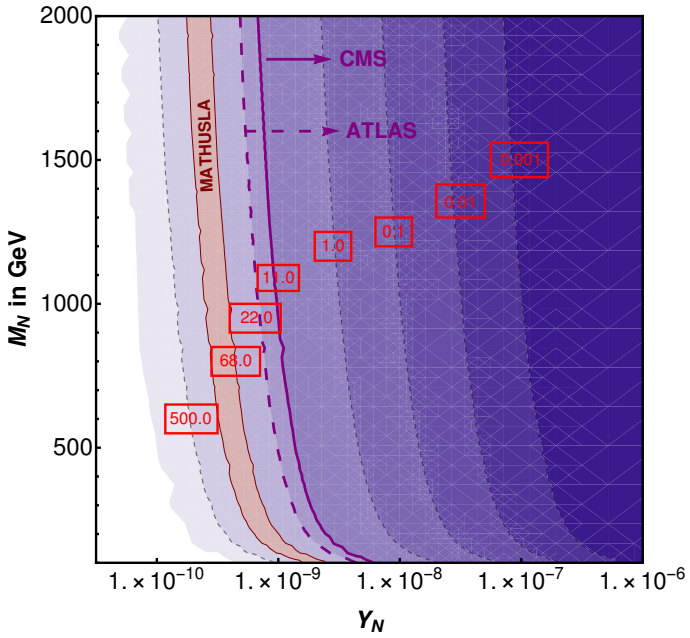

Figure 8. The displaced decay length of RHN is presented in $Y_N - M_N$ plane. Different regions of decay length from 0.001 m to 500 m are marked with red boxes. The CMS, ATLAS and MATHUSLA boundaries are shown in magenta solid, magenta dashed and brown thick lines, respectively.

and ATLAS boundaries in the longitudinal direction are shown with black dotted-dashed and dashed lines, respectively, while the corresponding boundary for the proposed FCC-hh reference detector is specified with blue dashed line. The regions for MATHUSLA is exhibited in the light-blue band. The golden yellow strip depicts the tiny region that can be explored by the FASER-II detector. The transverse regions also can be read from the figure 9, however the detector ranges are not shown explicitly in the figures.

In figure 9 (a, b, c), we have presented the transverse and longitudinal decay length distributions of BP1 ($M_N = 10\,\text{GeV}$). Because of the low Yukawa coupling and low mass, the decay length reaches up to 100 km in both the directions for 14 TeV centre of mass energy. Since the boost effect is stronger in the longitudinal direction compared to the transverse one, we can see the enhancement of decay length in the longitudinal direction for 27 and 100 TeV centre of mass energies(second and third columns). Due to the large decay lengths in BP1, most of the events fall outside the reach of CMS, ATLAS or MATHUSLA detectors. On the contrary, BP2 ($M_N = 60\,\text{GeV}$) is the most suitable to be detected by all three detectors simultaneously. Here the transverse and longitudinal decay length distributions for BP2 are depicted by figure 9 (d, e, f). Though the rest mass decay length for this benchmark point is around 4 meter (table 6), the displaced longitudinal decay length can reach up to 1 km for 100 TeV centre of mass energy due to the larger boost. Finally, the displaced transverse and longitudinal decay length distribution for BP3 ($M_N = 100\,\text{GeV}$) are shown in figure 9 (g, h, i). Here the maximum displacement can occur around 10 meters, resulting from all of the events inside the CMS, ATLAS or the proposed FCC-hh reference detector. We would like to mention that due to very small detectable

JHEP02(2023)103

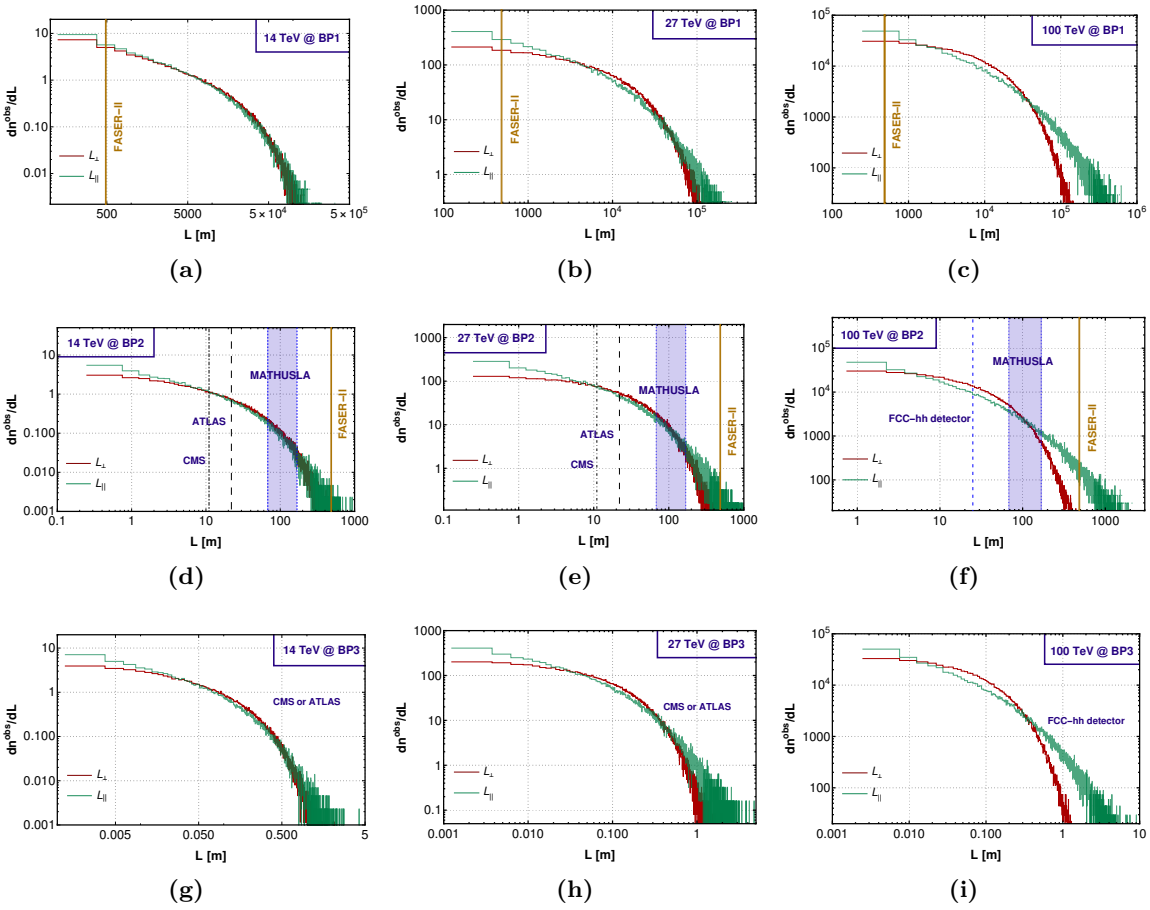

Figure 9. Displaced transverse ($L_\perp$ in red) and longitudinal ($L_{||}$ in green) decay length distributions for N, coming from the pair productions at the LHC with the centre of mass energies of 14 TeV (a, d, g), 27 TeV (b, e, h) and 100 TeV (c, f, i) for the integrated luminosities of 3, 10 and 30 ab^{-1}, respectively. The first, second and third rows delineate the distributions for BP1, BP2 and BP3, respectively. The black dotted-dashed and dashed lines indicate the upper limit of CMS and ATLAS, respectively, whereas, the blue dashed line specify the upper limit of the proposed FCC-hh detector. The light blue band (68 m−168 m) denotes the MATHUSLA region and the golden yellow strip denotes the FASER-II region. All of the regions depicted here are in the longitudinal direction.

range for the FASER-II, the event numbers are abysmally low even though they fall under the detectable ranges for BP1, BP2.

Table 7 presents the inclusive number of events that can be obtained inside MATHUSLA for BP2 with 14, 27 and 100 TeV centre of mass energies, at an integrated luminosity of 3 ab^{-1}, 10 ab^{-1} and 30 ab^{-1}, respectively. BP1 and BP3 are beyond the reach of MATHUSLA; former having the decay length beyond the reach and the later having them within the range of 10 m.

JHEP02(2023)103

	Events inside MATHUSLA		
	Centre of mass energy		
	14 TeV	27 TeV	100 TeV
BP2	4.7	385.7	38029.2

Table 7. The inclusive number of events inside the proposed detector, MATHUSLA, for the second benchmark point (BP2), at the centre of mass energies of 14, 27 and 100 TeV at an integrated luminosity of $3\,\text{ab}^{-1}$, $10\,\text{ab}^{-1}$ and $30\,\text{ab}^{-1}$, respectively.

Displaced decay / 4ℓ	Benchmark points	Centre of mass energy		
		14 TeV	27 TeV	100 TeV
CMS	BP1	0.0	0.4	—
	BP2	0.5	33.2	—
	BP3	2.6	196.3	—
ATLAS & FCC-hh reference detector	BP1	0.0	0.6	17.7
	BP2	0.7	49.4	4393.44
	BP3	2.6	196.3	17032.68
MATHUSLA	BP1	0.0	0.3	33.7
	BP2	0.0	3.2	236.52
	BP3	0.0	0.0	0.0

Table 8. Number of events in 4ℓ final state for the benchmark points with the center of mass energies of 14 TeV, 27 TeV and 100 TeV at the integrated luminosities of $3\,\text{ab}^{-1}$, $10\,\text{ab}^{-1}$ and $30\,\text{ab}^{-1}$, respectively. The numbers are given separately for CMS, ATLAS, FCC-hh reference detector (for 100 TeV) and MATHUSLA.

3.5 Number of displaced leptonic events

In this section, we present the number of displaced leptonic events collected by the CMS, ATLAS and MATHUSLA detectors for 14 and 27 TeV colliders. As the detector specifications change from 14 TeV to 100 TeV, we provide the number of events with FCC-hh reference detector at 100 TeV (specified earlier) and MATHUSLA, taking into account the larger forward cover of the projected detector shape.

RHNs produced via Z_{B-L} has dominant decays to $\ell^{\pm}W^{\mp}$ for the chosen benchmark points. Thus multi-leptonic final states are mostly common, when the gauge bosons also decay leptonically. In the following tables we present the final state numbers coming from different multi-leptonic final state topologies.

Four lepton final states can arise from leptonic decays of both the $W^{\pm}$s or one of the Z bosons coming from the RHN. In table 8, we present the number of inclusive 4ℓ final state which are displaced for the chosen benchmark points for the centre of mass energies of 14, 27 and 100 TeV, at an integrated luminosities of 3, 10 and 30 ab^{-1}, respectively.

JHEP02(2023)103

Displaced decay / $3\ell + (\geq 1j)$	Benchmark points	Centre of mass energy		
		14 TeV	27 TeV	100 TeV
CMS	BP1	0.0	0.6	—
	BP2	1.9	88.7	—
	BP3	5.4	383.8	—
ATLAS & FCC-hh reference detector	BP1	0.0	0.8	41.8
	BP2	2.3	121.3	10872.4
	BP3	5.4	383.8	35228.0
MATHUSLA	BP1	0.0	0.5	60.5
	BP2	0.1	5.3	635.0
	BP3	0.0	0.0	0.0

Table 9. Number of events in $3\ell + (\geq 1j)$ final state for the benchmark points with the center of mass energies of 14 TeV, 27 TeV and 100 TeV at the integrated luminosities of $3\,\text{ab}^{-1}$, $10\,\text{ab}^{-1}$ and $30\,\text{ab}^{-1}$, respectively. The numbers are given separately for CMS, ATLAS, FCC-hh reference detector (for 100 TeV) and MATHUSLA.

The 4ℓ final states are generally with very little SM backgrounds, especially after the reconstruction of the RHN invariant mass. In this case due to the displaced vertex signatures the final state is background free. We also segregate the event numbers for the CMS, ATLAS and MATHUSLA detectors. It is interesting to note that for BP1 ($M_N = 10\,\text{GeV}$), the rest mass decay length is 193 m, which is already out of the ranges of CMS, ATLAS and MATHUSLA and thus boost effect further makes it undetectable. As mentioned earlier in the text, for BP2 all three detectors fall in the regions of the displaced decays specially for 27, 100 TeV centre of mass energies, however, for BP3, the displaced decay lengths are restricted to CMS and ATLAS and fails to reach in the MATHUSLA range.

After 4ℓ signature we move to $3\ell + (\geq 1j)$ signature, which results in when one of the gauge boson decays hadronically, as we present the numbers in table 9. The inclusive $3\ell + (\geq 1j)$ numbers are predicted for the LHC/FCC with centre of mass energy of 14, 27 and 100 TeV at an integrated luminosities of $3\,\text{ab}^{-1}$, $10\,\text{ab}^{-1}$ and $30\,\text{ab}^{-1}$, respectively. For CMS and ATLAS only BP2 and BP3 have healthy event numbers. MATHUSLA fails to register any significant event numbers for all three benchmark points, except for BP2 at higher energies.

In table 10, we describe the event numbers for $2\ell + (\geq 2j)$ final state for the benchmark points with the center of mass energies of 14 TeV, 27 TeV and 100 TeV at the integrated luminosities of $3\,\text{ab}^{-1}$, $10\,\text{ab}^{-1}$ and $30\,\text{ab}^{-1}$, respectively. Unlike earlier two final states, here we have significant number of events for BP1 and BP2 for higher energies. For CMS and ATLAS, BP2 and BP3 can be probed very easily. Due to highest branching fraction of $W^{\pm}$ to hadronic mode and because of the Fatjet signature, the event numbers for $2\ell + \geq 2j$ are largest for all the benchmark points.

JHEP02(2023)103

Displaced decay / $2\ell + (\geq 2j)$	Benchmark points	Centre of mass energy		
		14 TeV	27 TeV	100 TeV
CMS	BP1	0.0	2.3	—
	BP2	7.5	442.2	—
	BP3	14.1	1066.7	—
ATLAS & FCC-hh reference detector	BP1	0.1	3.4	308.7
	BP2	9.8	623.7	57844.8
	BP3	14.1	1066.7	102492.2
MATHUSLA	BP1	0.0	5.3	443.9
	BP2	0.4	30.3	3354.2
	BP3	0.0	0.0	0.0

Table 10. Number of events in $2\ell + (\geq 2j)$ final state for the benchmark points with the center of mass energies of 14 TeV, 27 TeV and 100 TeV at the integrated luminosities of $3\,\text{ab}^{-1}$, $10\,\text{ab}^{-1}$ and $30\,\text{ab}^{-1}$, respectively. The numbers are given separately for CMS, ATLAS, FCC-hh reference detector (for 100 TeV) and MATHUSLA.

3.6 Sensitivity regions at different energies

The dominant decay mode of a single RHN is $N \to W^{\pm}\ell^{\mp}$, which gives $1\ell + 2j$ signature, results in the RHN pair with $2\ell + 4j$ final state. However, for the lower RHN mass, due to the large boost, the two-jets coming from the on- or off-shell $W^{\pm}$ boson are collimated to form a single Fatjet even with the jet radius of 0.5, catalyses the final state of $2\ell + 2j$ as we elaborate in the following paragraphs.

In this section, we draw the sensitivity regions in the $M_{Z_{B-L}} - M_N$ plane at the LHC/FCC with centre of mass energies of 14, 27, 100 TeV for 2ℓ+$2j$ final state (dark shaded region) and for $2\ell + 4j$ final state (light shaded region). Here we follow the prescription of Poisson distribution in order to estimate the 95% confidence level sensitivity plots for the non-observation of signals [73, 74] with zero backgrounds.

In figure 10, we plot the regions in the $M_{Z_{B-L}} - M_N$ plane which can be probed at 95% confidence levels with the centre of mass energies of 14 TeV, 27 TeV and 100 TeV at the integrated luminosities of 1 (3), 6 (10), and 15 (30) ab^{-1}, respectively. These regions include two different final state topologies: the darker green (darker brown) corresponds to $2\ell + 2j$ and the lighter green (lighter brown) refers to $2\ell + 4j$ final state. For lower RHN mass ($\lesssim 250$ GeV for 14 TeV centre of mass energy), Fatjets forms and thus the final state of $2\ell + 2j$ occurs more often than $2\ell + 4j$, which is more probable for higher RHN mass as discussed in subsection 3.3. Such analysis shows that a very light RHN i.e. $M_N \sim 30$ GeV can be probed along with $M_{Z_{B-L}} \sim 7$ TeV for 14 TeV centre of mass energy. However, at 100 TeV, a very low RHN mass of ~ 5 GeV can be probed along with a maximum of 900 GeV and $M_{Z_{B-L}} \sim 15.5$ TeV. For very low RHN masses, the decay widths become small, resulting in a very long displaced decay length which is outside any of the detectors.

JHEP02(2023)103

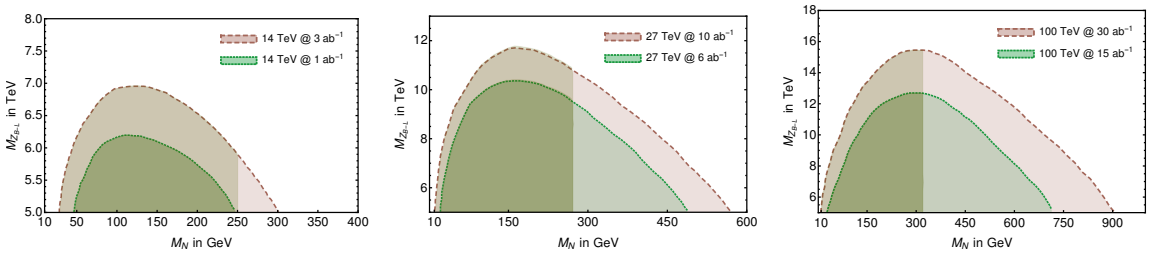

(a) (b) (c)

Figure 10. Limits obtained via the inclusive measurements from RHNs decay to displaced $2\ell + 2j$ final state (dark shaded region), displaced $2\ell + 4j$ final state (light shaded region) and it is presented in $M_{Z_{B-L}}$ versus M_N plane at 95% CL. The shaded regions can be probed at any of the detectors CMS, ATLAS and MATHUSLA for 14, 27 TeV centre of mass energies, and at either of the FCC-hh reference detector and MATHUSLA for 100 TeV centre of mass energy, considering the root sum square values of the Yukawa couplings discussed in subsection 3.1.

4 Scenario-2

In this scenario, we focus on the case where one of the RHNs decouples from the observed neutrino mass generations, with the possibility of much smaller Yukawa coupling, while the rest two can explain light neutrino masses and mixing. Thus collider predictions here is solely for one generation of RHN.

4.1 Parameter space and benchmark points

Scenario-2 assumes the presence of a RHN which couples dominantly to electron or muon and whose Yukawa coupling is too small to produce a sizeable neutrino mass scale. This implies that the observed neutrino mass matrix is generated by the other two RHNs. We further assume that they do not produce displaced vertices. For the analysis of this scenario, we take two benchmark points: BP2 ($M_N = 60\,\text{GeV}$) and BP3 ($M_N = 100\,\text{GeV}$) with two different values of the Yukawa coupling: $Y_N = 5 \times 10^{-8}$ and 5×10^{-9}.

4.2 Displaced vertex signatures

Repeating the previous analyses for this scenario, we obtain figure 11, which describes the differential distribution of displaced decay lengths for the benchmark points at 14, 27 and 100 TeV centre of mass energies with the integrated luminosities of 3, 10, 30 ab^{-1}, for $Y_N = 5 \times 10^{-8}$ and 5×10^{-9}. Figure 11(a, b, c) depict the distributions for BP2 with $Y_N = 5 \times 10^{-8}$ and it can be noticed that the displaced decay lengths can reach to 10 km for both transverse ($L_\perp$) and longitudinal ($L_{||}$) ones. The corresponding inclusive event numbers, that fall inside the MATHUSLA detector, are given in table 11 (first row), at the centre of mass energies of 14, 27 and 100 TeV with the integrated luminosities of $3\,\text{ab}^{-1}$, $10\,\text{ab}^{-1}$ and $30\,\text{ab}^{-1}$, respectively. Figure 11(d, e, f) present the corresponding distributions for BP3 and since the displaced decay lengths are mostly less than 100 m, at least for

JHEP02(2023)103

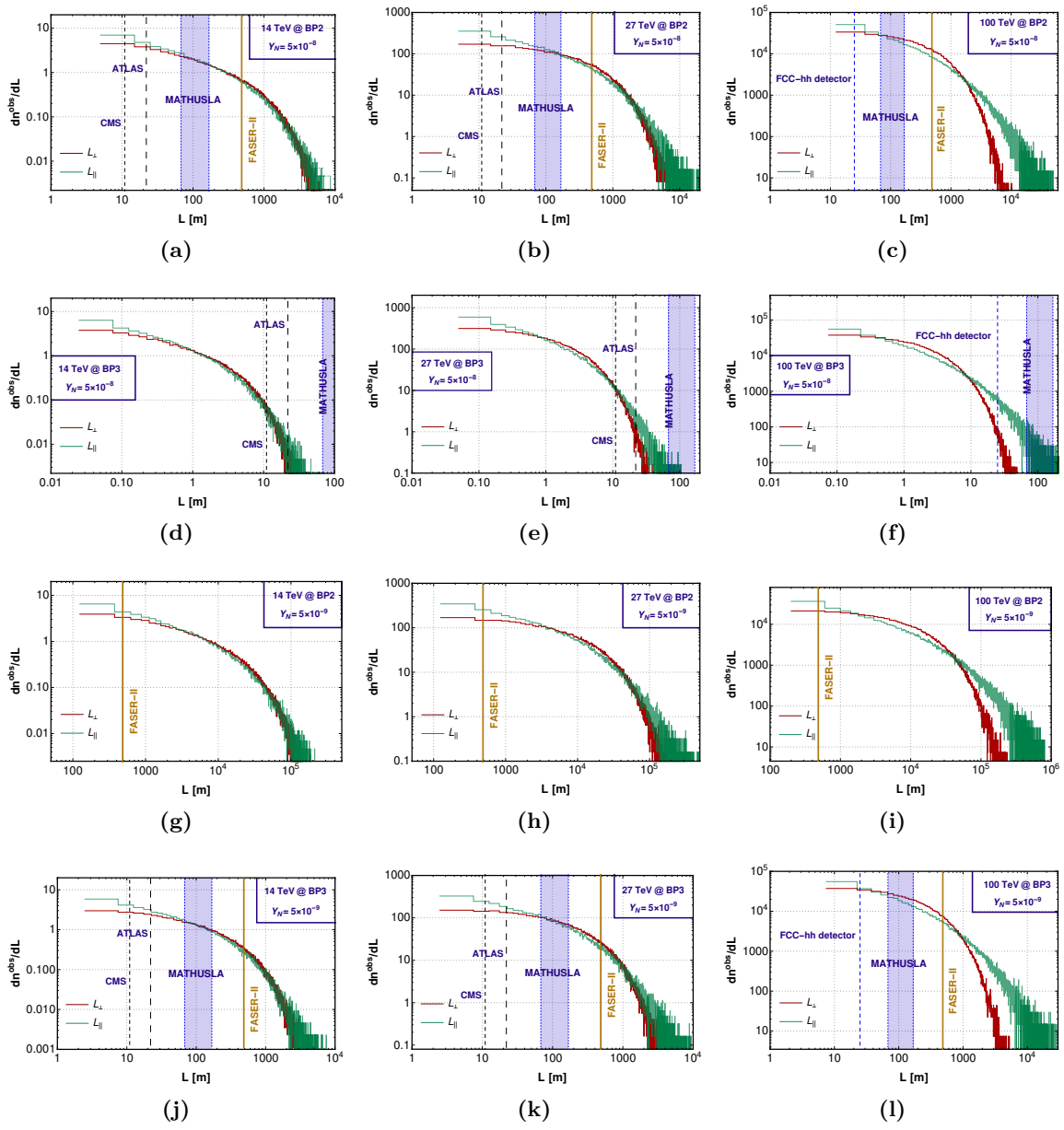

Figure 11. Displaced transverse ($L_\perp$ in red) and longitudinal ($L_{||}$ in green) decay length distributions for N, coming from the pair productions at the LHC with the centre of mass energies of 14 TeV (a, d, g, j), 27 TeV (b, e, h, k) and 100 TeV (c, f, i, l) with the integrated luminosities of 3, 10, 30 ab^{-1}, respectively for BP2 (first, third rows) and BP3 (second, fourth rows). The choice of Yukawa couplings are $Y_N = 5 \times 10^{-8}$ (first, second rows) and $Y_N = 5 \times 10^{-9}$ (third, fourth rows). The small-dashed and medium-dashed lines indicate the upper limits of CMS and ATLAS, respectively, whereas, the blue dashed line specify the upper limit of the proposed FCC-hh detector. The light blue band (68 m−168 m) denotes the MATHUSLA region and the golden yellow strip denotes the FASER-II region.

JHEP02(2023)103

Yukawa coupling	Benchmark points	Events inside MATHUSLA		
		Centre of mass energy		
		14 TeV	27 TeV	100 TeV
5×10^{-8}	BP2	1.4	81.2	6013.4
	BP3	0.0	1.7	534.2
5×10^{-9}	BP2	0.5	3.8	53.3
	BP3	1.6	113.1	8645.8

Table 11. The inclusive number of events inside the proposed detector MATHUSLA, for BP2 and BP3, with the Yukawa couplings of 5×10^{-8}, 5×10^{-9}, at the centre of mass energies of 14, 27, 100 TeV with the integrated luminosities of $3\,\text{ab}^{-1}$, $10\,\text{ab}^{-1}$ and $30\,\text{ab}^{-1}$, respectively.

$L_\perp$, numbers are negligible. However, due to large longitudinal boost at 100 TeV, the corresponding distribution reaches MATHUSLA region and the number is also encouraging (table 11 second row).

Figure 11(g, h, i) and figure 11(j, k, l) show the distributions for BP2 and BP3, respectively with $Y_N = 5 \times 10^{-9}$. This enhances the displacement, and thus we have more events for BP3 as can be read from table 11 (fourth row). For BP2, the displacements reaches up to $\sim 10^5$ m leaving very little events inside MATHUSLA range. We also depict the FASER-II regions, but FASER-II prospect is not encouraging due to very small range in this model.

4.3 Number of displaced leptonic events

Let us now present the event numbers for the final states of displaced 4ℓ, $3\ell + 1j$ and $2\ell + 2j$ at the center of mass energies of 14 TeV, 27 TeV and 100 TeV with the integrated luminosities of $3\,\text{ab}^{-1}$, $10\,\text{ab}^{-1}$ and $30\,\text{ab}^{-1}$, respectively. Table 12 shows the numbers of 4ℓ events. It is evident that CMS, ATLAS and the proposed detector for FCC-hh can have healthy event numbers only for BP3 at higher centre of mass energies of 27 and 100 TeV. MATHUSLA registers some good number of events for BP3 with $Y_N = 5 \times 10^{-9}$ at 100 TeV. For BP2 the event numbers remain low at all three detectors as compared to BP3.

Next, we indulge in the final state of $3\ell + (\geq 1j)$ shown in table 13. Similarly to the 4ℓ final state, the events numbers are healthy only for BP3 at 27 and 100 TeV centre of mass energies. BP2 looks promising only for $Y_N = 5 \times 10^{-8}$ at 100 TeV.

Finally the results for the final state of $2\ell + (\geq 2j)$ are presented in table 14. Overall event numbers are comparatively healthy for both the benchmark points. However, MATHUSLA is favorable to BP2 with $Y_N = 5 \times 10^{-8}$ and BP3 with $Y_N = 5 \times 10^{-9}$ for 100 TeV centre of mass energy.

4.4 Sensitivity regions at different energies

In the scenario-2, only one RHN having a very small Yukawa coupling is responsible for the displaced decay phenomenology. The other two can have relatively larger Yukawa couplings while reproducing the observed neutrino masses and mixing [75]. Figure 12

JHEP02(2023)103

Displaced decay / 4ℓ	Yukawa couplings (Y_N)	Benchmark points	Centre of mass energy		
			14 TeV	27 TeV	100 TeV
CMS	5×10^{-8}	BP2	0.0	2.7	—
		BP3	1.8	129.4	—
	5×10^{-9}	BP2	0.0	0.0	—
		BP3	0.1	7.3	—
ATLAS & FCC-hh reference detector	5×10^{-8}	BP2	0.1	3.6	292.32
		BP3	1.9	133.7	12566.8
	5×10^{-9}	BP2	0.0	0.0	4.1
		BP3	0.2	12.9	1082.2
MATHUSLA	5×10^{-8}	BP2	0.0	1.5	90.5
		BP3	0.0	0.3	12.6
	5×10^{-9}	BP2	0.0	0.1	3.2
		BP3	0.0	3.0	209.1

Table 12. Number of events in 4ℓ final state for the benchmark points, corresponds to the Yukawa couplings ($Y_N =$) 5×10^{-8} and 5×10^{-9}, with the center of mass energies of 14 TeV, 27 TeV and 100 TeV at the integrated luminosities of $3\,\text{ab}^{-1}$, $10\,\text{ab}^{-1}$ and $30\,\text{ab}^{-1}$, respectively. The numbers are given separately for CMS, ATLAS, FCC-hh reference detector (for 100 TeV) and MATHUSLA.

Displaced decay / $3\ell + (\geq 1j)$	Yukawa couplings (Y_N)	Benchmark points	Centre of mass energy		
			14 TeV	27 TeV	100 TeV
CMS	5×10^{-8}	BP2	0.2	5.7	—
		BP3	3.2	195.3	—
	5×10^{-9}	BP2	0.0	0.1	—
		BP3	0.4	14.2	—
ATLAS & FCC-hh reference detector	5×10^{-8}	BP2	0.3	8.6	620.1
		BP3	3.3	199.3	17121.7
	5×10^{-9}	BP2	0.0	0.2	25.2
		BP3	0.6	23.1	1691.6
MATHUSLA	5×10^{-8}	BP2	0.0	1.7	134.1
		BP3	0.0	0.5	33.6
	5×10^{-9}	BP2	0.0	0.3	16.8
		BP3	0.1	4.4	306.6

Table 13. Number of events in $3\ell + (\geq 1j)$ final state for the benchmark points, corresponds to the Yukawa couplings $Y_N = 5 \times 10^{-8}$ and 5×10^{-9}, with the center of mass energies of 14 TeV, 27 TeV and 100 TeV at the integrated luminosities of $3\,\text{ab}^{-1}$, $10\,\text{ab}^{-1}$ and $30\,\text{ab}^{-1}$, respectively. The numbers are given separately for CMS, ATLAS, FCC-hh reference detector (for 100 TeV) and MATHUSLA.

JHEP02(2023)103

Displaced decay / $2\ell + (\geq 2j)$	Yukawa couplings (Y_N)	Benchmark points	Centre of mass energy		
			14 TeV	27 TeV	100 TeV
CMS	5×10^{-8}	BP2	0.6	20.7	—
		BP3	5.1	303.0	—
	5×10^{-9}	BP2	0.0	0.8	—
		BP3	0.7	25.3	—
ATLAS & FCC-hh reference detector	5×10^{-8}	BP2	0.9	33.8	2546.2
		BP3	5.2	309.3	28186.1
	5×10^{-9}	BP2	0.0	1.8	232.2
		BP3	1.0	40.4	2901.5
MATHUSLA	5×10^{-8}	BP2	0.2	9.2	795.6
		BP3	0.0	0.8	49.5
	5×10^{-9}	BP2	0.0	1.2	62.7
		BP3	0.1	6.7	553.3

Table 14. Number of events in $2\ell + (\geq 2j)$ final state for the benchmark points, corresponds to the Yukawa couplings ($Y_N =$) 5×10^{-8} and 5×10^{-9}, with the center of mass energies of 14 TeV, 27 TeV and 100 TeV at the integrated luminosities of $3\,\text{ab}^{-1}$, $10\,\text{ab}^{-1}$ and $30\,\text{ab}^{-1}$, respectively. The numbers are given separately for CMS, ATLAS, FCC-hh reference detector (for 100 TeV) and MATHUSLA.

describes the reaches in the $M_N - M_{Z_{B-L}}$ plane for three different centre of mass energies 14, 27 and 100 TeV. The colour conventions are same as in figure 10, however we have chosen $Y_N = 5 \times 10^{-8}$ for the first row and $Y_N = 5 \times 10^{-9}$ for the second row, respectively. It can be seen that the reach for M_N has increased substantially as compared to figure 10 due to the smaller Yukawa couplings.

For $Y_N = 5 \times 10^{-8}$ (in figure 12 first row) M_N can be probed up to 1.15 TeV, while Z_{B-L} reach can be up to 7.3 TeV at 14 TeV centre of mass energy. At 100 TeV, these are enhanced to 3.75 TeV, and 30 TeV, respectively. The reach on the lower end of M_N is 10 GeV, which is a little high as compare to figure 10. The results for $Y_N = 5 \times 10^{-9}$ are shown in the second row of figure 12. The choice of lower Yukawa pushed the probable regions towards the right side, i.e. for higher M_N. The maximum values that can be explored are $M_N = 1.42\,(4.18)$ TeV and $M_{Z_{B-L}} = 7.4\,(30.5)$ TeV at 14 (100) TeV centre of mass energy.

As the Yukawa coupling Y_N can be arbitrarily small in the scenario-2, it is also interesting to see how small Y_N can be probed by the displaced events. In figure 13 we show the regions in $Y_N - M_{Z_{B-L}}$ plane, that can be probed by different detectors at the LHC/FCC for centre of mass energies of 14, 27 and 100 TeV with 3, 10 and 30 ab^{-1} luminosities, respectively. For this we choose the mass ratio: $M_{Z_{B-L}} = 10 M_N$, and consider the $2\ell + 4j$ final state. The purple, pink and brown colours depict the regions that can be probed by CMS, ATLAS and MATHUSLA via the displaced decays, whereas, the grey regions repre-

JHEP02(2023)103

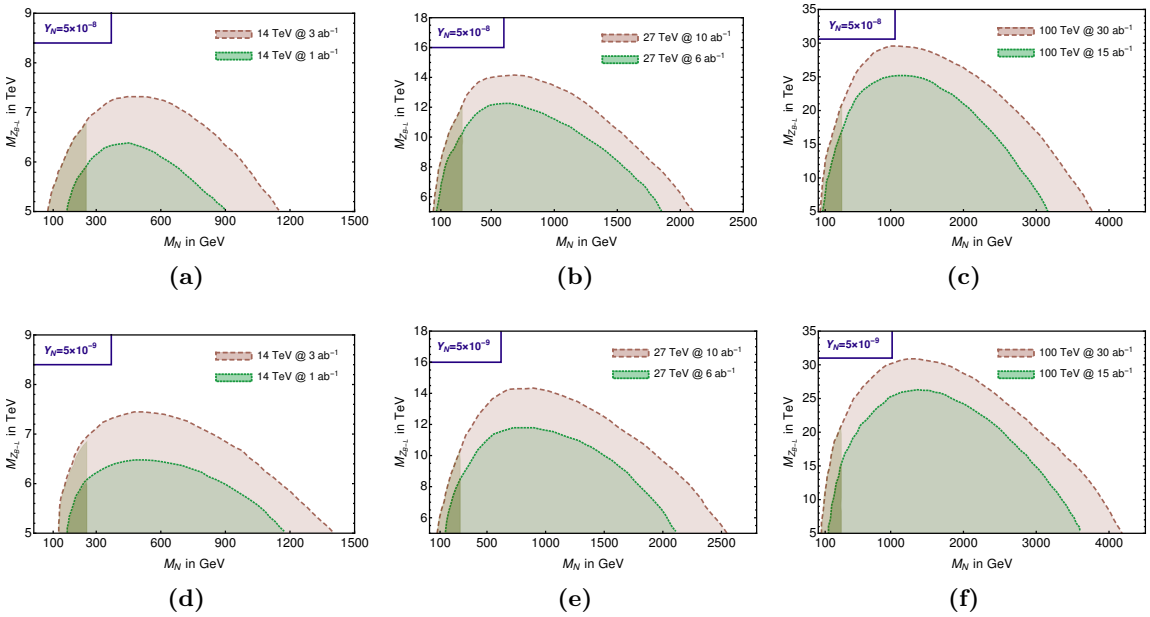

Figure 12. Limits obtained via the displaced decays of RHNs to $2\ell + 2j$ final state (dark shaded region), $2\ell + 4j$ final state (light shaded region) and it is presented in $M_{Z_{B-L}}$ versus M_N plane at 95% CL. The first and second panel present the probable regions for the Yukawa couplings 5×10^{-8} and 5×10^{-9}, respectively. The shaded regions can be probed at any of the detectors CMS, ATLAS and MATHUSLA for 14 TeV (a, d), 27 TeV (b, e) centre of mass energies, and at either of the FCC-hh reference detector and MATHUSLA for 100 TeV (c, f) centre of mass energy.

sent the same for the proposed FCC-hh detector. Such detectability via different detectors have overlapping regions also as can be seen from figure 13. MATHUSLA is $\mathcal{O}(100\,\text{m})$ from the interaction point and more sensitive for lower Y_N, as decay length varies inversely with Y_N. In the figure, one can see that $Y_N \sim 3 \times 10^{-12} - 10^{-6}$ can be probed combining the proposed FCC-hh detector and MATHUSLA for 100 TeV centre of mass energy via displaced decay. The corresponding reach for $M_{Z_{B-L}}$ is around 7.2 (33) TeV for 14 (100) TeV centre of mass energies considering the chosen mass hierarchy and the mentioned final state.

In the similar manner, the parameter space can be explored in a different angle. In figure 14, the reaches in the $Y_N - M_N$ plane are shown for a fixed value of $M_{Z_{B-L}} = 5$ TeV. We present our result in a log-log scale for $2\ell+2j$ final state with darker shades, and $2\ell+4j$ with lighter shades with the centre of mass energies of 14, 27, 100 TeV at the luminosities of 3, 10, 30 ab^{-1}, respectively. The pink, blue and brown regions can be explored by ATLAS, CMS and MATHUSLA, respectively, whereas, the grey region can be probed via FCC-hh reference detector described in subsection 3.4. As the cross-section decreases with the increase of the RHN mass, the reach stays up to $M_N = 2.5\,(10)$ TeV for 14 (100) TeV centre of mass energies at the LHC (FCC-hh). Displaced decay can be observed for the RHN mass of ~ 3 GeV with substantially high Yukawa coupling up to $\sim 10^{-3}$.

JHEP02(2023)103

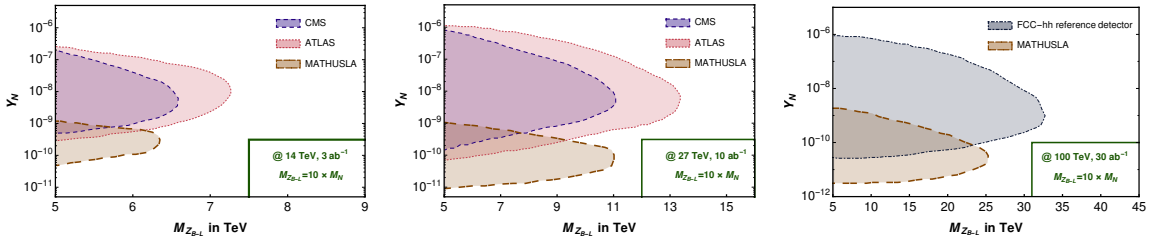

Figure 13. Limits obtained via the displaced decays of RHNs to $2\ell+4j$ final state and is presented in Y_N versus $M_{Z_{B-L}}$ plane at 95% CL, where $M_{Z_{B-L}} = 10M_N$. The probable regions are shown for different centre of mass energies, i.e. 14 TeV, 27 TeV and 100 TeV with the integrated luminosities of 3, 10 and 30 ab^{-1}, respectively. The purple, pink, grey and light brown colours depict the reaches for CMS, ATLAS, FCC-hh reference detector and MATHUSLA, respectively.

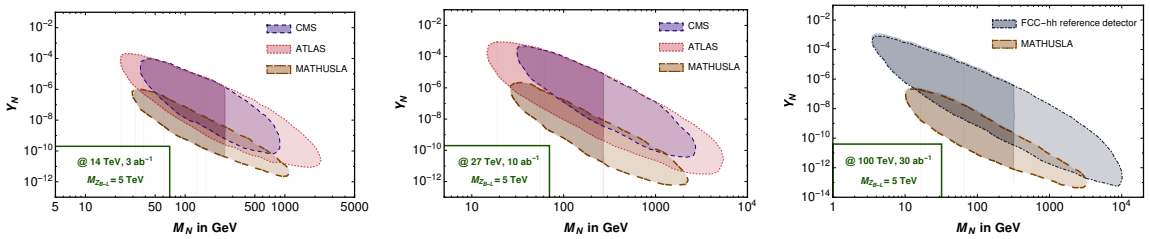

Figure 14. Limits obtained via the displaced decays of RHNs to $2\ell + 2j$ final state (dark shaded region), $2\ell + 4j$ final state (light shaded region) and it is presented in Y_N versus M_N plane at 95% CL, where $M_{Z_{B-L}}$ is 5 TeV. The probable regions are for different centre of mass energies, i.e. 14 TeV, 27 TeV and 100 TeV at the integrated luminosities of 3, 10 and 30 ab^{-1}, respectively. The purple, pink, grey and light brown colours depict the reaches for CMS, ATLAS, FCC-hh reference detector and MATHUSLA, respectively.

5 Boost effect on di-lepton final state

In this section we investigate the boost effect to our most desired final states of two leptons, which arise as $2\ell + 2j$ and $2\ell + 4j$. 2ℓ final state can come from the leptonic decays of the gauge bosons. In case of leptons coming from Z boson, it gives rise to final states with opposite sign lepton and maximally two parton level jets. However, if we focus on the scenario where both the RHNs decay via $\ell^{\pm}W^{\mp}$, it gives rise to final state of $2\ell + 4j$ (if the $W^{\mp}$ decays hadronically), where the leptons can be either same sign or opposite sign and ideally with 1:1 ratio. The departure from the ideal case happens when the mass of the RHN is smaller as compared to the centre of mass energy of the collider, producing boosted RHNs. In that case two of the potential jets coming from the $W^{\pm}$, are collimated and form a Fatjet and we obtain $2\ell + 2j$ final state.

The leptons coming from two RHNs decay can give rise to same sign di-lepton and opposite sign di-lepton and N being Majorana in nature the ratio of SS:OS ideally should be

JHEP02(2023)103

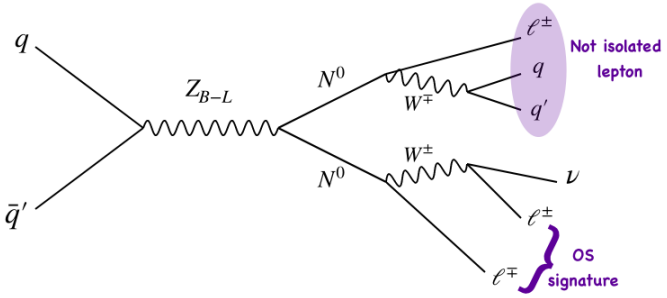

Figure 15. A schematic diagram of getting more OS over SS in boosted scenario.

	Final states	M_N in GeV	Centre of mass energy			
			27 TeV		100 TeV	
			SS	OS	SS	OS
CMS	$2\ell+2j$	60	15.6 (5.3%)	273.9 (94.7%)	—	—
		100	87.7 (10.2%)	768.3 (89.7%)	—	—
		250	231.4 (17.7%)	1085.3 (82.4%)	—	—
	$2\ell+4j$	500	54.7 (20.5%)	211.4 (79.4%)	—	—
ATLAS & FCC-hh reference detector	$2\ell+2j$	60	29.5 (6.1%)	453.1 (93.9%)	2057.9 (4.3%)	45510.6 (95.7%)
		100	87.7 (10.2%)	768.3 (89.7%)	7582.7 (9.3%)	73820.1 (90.7%)
		250	231.4 (17.7%)	1085.3 (82.4%)	8011.4 (22.4%)	27726.6 (77.6%)
	$2\ell+4j$	500	54.7 (20.5%)	211.4 (79.4%)	566.8 (23.0%)	1893.3 (76.9%)
MATHUSLA	$2\ell+2j$	60	1.8 (7.3%)	22.9 (92.7%)	258.3 (9.4%)	2461.7 (90.6%)
		100	—	—	—	—
		250	—	—	—	—
	$2\ell+4j$	500	—	—	—	—

Table 15. Number of events containing SS or OS and their percentage numbers (in bracket) for different RHN masses (M_N in GeV) with the centre of mass energies of 27, 100 TeV, at the integrated luminosities of 10, 30 ab^{-1}, respectively, considering the root sum square values of the Yukawa couplings discussed in subsection 3.1.

1:1 [76–78]. Such signature can be achieved if we demand both the $W^\pm$s coming from two RHNs decays hadronically and thus having a parton level final state of $2\ell + 4j$. However, the lepton coming from RHN decays often are co-linear to the hadronic jet coming from the $W^\pm$ decays and thus cannot satisfy the isolation criteria, whereas, we still get di-lepton when the other $W^\pm$ from the other RHN decays leptonically as can be seen from figure 15. In that case the second RHN leg fully contribute to di-lepton, which only contributes to OS and other ISR/FSR jets add up to the $4j$ criteria. In the absence of the hard ISR/FSR jets satisfying the cuts (subsection 3.2), such events forms a final state of $2\ell+2j$ and more likely to happen for lighter RHNs ($M_N \lesssim 300$ GeV). However, for higher M_N ($gtrsim300$ GeV), $2\ell+4j$ final state is more likely. These two phenomena are explicitly mentioned in table 15 and table 16. In both the cases, such collinearity leads to skewed ratio of SS:OS, and as we go for higher mass values, the ratio of SS:OS gets better.

JHEP02(2023)103

	Final states	M_N in GeV	Centre of mass energy			
			27 TeV		100 TeV	
			SS	OS	SS	OS
CMS	$2\ell+2j$	100	3.2 (15.4%)	17.6 (84.6%)	—	—
		250	10.3 (26.3%)	28.8 (73.6%)	—	—
	$2\ell+4j$	500	16.1 (32.6%)	33.3 (67.4%)	—	—
		1000	13.5 (34.4%)	25.8 (65.6%)	—	—
ATLAS & FCC-hh reference detector	$2\ell+2j$	100	5.6 (16.0%)	29.3 (83.9%)	397.8 (18.2%)	1781.6 (81.8%)
		250	13.1 (25.2%)	38.8 (74.7%)	623.2 (27.4%)	1653.8 (72.6%)
	$2\ell+4j$	500	18.4 (32.7%)	37.7 (67.2%)	702.0 (36.7%)	1208.4 (63.2%)
		1000	14.4 (34.6%)	27.2 (65.4%)	547.7 (37.8%)	899.9 (62.1%)
MATHUSLA	$2\ell+2j$	100	0.7 (15.2%)	3.9 (84.7%)	73.9 (14.8%)	422.1 (85.1%)
		250	1.6 (23.5%)	5.2 (76.3%)	84.2 (22.9%)	282.5 (77.1%)
	$2\ell+4j$	500	1.5 (34.8%)	2.8 (65.1%)	13.1 (25.2%)	38.8 (74.7%)
		1000	—	—	—	—

Table 16. Number of events containing SS or OS and their percentage numbers (in bracket) for different RHN masses (M_N in GeV) with the centre of mass energies of 27, 100 TeV, at the integrated luminosities of 10, 30 ab^{-1}, respectively, and for $Y_N = 5 \times 10^{-9}$.

Scenario-1 (section 3) deals with $U_{\rm PMNS}$ with three generations of RHNs in Casas-Ibarra parameterization, where $Y_N \sim \sqrt{M_N}$, that leads to relatively higher Y_N for higher mass values. In table 15 we present the number of events for $2\ell + 2j$ final state for $M_N =$ 60, 100, 250, 500 GeV. The events for $M_N = 10$ GeV are mostly outside the detectors i.e. CMS, ATLAS, FCC-hh reference detector and MATHUSLA. Whereas, for $M_N = 1000$ GeV, we get prompt leptons, which is not our interest for this article. $M_N = 60$ GeV, has some events for $2\ell + 2j$ final state inside MATHUSLA detectors, unlike 100, 250, 500 GeV, which lie inside the CMS, ATLAS or proposed FCC-hh reference detector range.

Table 16 describes the similar situation for the scenario-2 (in section 4), where we consider only one generations of RHN with $Y_N = 5 \times 10^{-9}$. In this case even for $M_N =$ 1000 GeV, we obtain the displaced signature for $2\ell + 4j$ final state. However, for $M_N =$ 1000 GeV point, the displaced decay does not reach to MATHUSLA.

It has been noted that without tagging the legs, i.e. the RHNs, event for higher mass values, it is not possible to get OS:SS as 1:1. Achieving Majorana nature thus relies on perfectly tagging of both the RHNs in a pair production which will be discussed in the next section.

6 Majorana nature: OSD vs SSD

To extract the information for the Majorana fermion, it is essential to reconstruct the RHNs, i.e. the legs from which the charged leptons are coming. Charged leptons coming from such RHNs, without the contamination of the leptons from the other gauge bosons in the decay chain can easily satisfy the same sign di-lepton (SSD): opposite sign di-lepton (OSD) equals to 1:1 [76–78]. It is worth mentioning here, since MATHUSLA will be

JHEP02(2023)103

	Final states	M_N in GeV	Centre of mass energy			
			27 TeV		100 TeV	
			SS	OS	SS	OS
CMS	$2\ell+2j$	100	23.8 (48.8%)	25.0 (51.2%)	—	—
		250	48.4 (49.0%)	50.3 (51.0%)	—	—
	$2\ell+4j$	500	16.6 (49.4%)	17.0 (50.6%)	—	—
ATLAS & FCC-hh reference detector	$2\ell+2j$	100	23.8 (48.8%)	25.0 (51.2%)	434.7 (49.2%)	448.4 (50.7%)
		250	48.4 (49.0%)	50.3 (51.0%)	549.5 (48.8%)	576.1 (51.2%)
	$2\ell+4j$	500	16.6 (49.4%)	17.0 (50.6%)	202.0 (49.6%)	205.6 (50.4%)

Table 17. Number of events containing SSD or OSD and their percentage numbers (in bracket) for different RHN masses (M_N in GeV) with the centre of mass energies of 27, 100 TeV, at the integrated luminosities of 10, 30 ab^{-1}, respectively, considering the root sum square values of the Yukawa couplings discussed in subsection 3.1.

	Final states	M_N in GeV	Centre of mass energy			
			27 TeV		100 TeV	
			SSD	OSD	SSD	OSD
CMS	$2\ell+2j$	100	2.6 (48.1%)	2.8 (51.8%)	—	—
		250	7.9 (49.0%)	8.2 (51.0%)	—	—
	$2\ell+4j$	500	12.9 (48.7%)	13.6 (51.3%)	—	—
		1000	10.1 (48.8%)	10.6 (51.2%)	—	—
ATLAS & FCC-hh reference detector	$2\ell+2j$	100	3.4 (48.6%)	3.6 (51.4%)	223.6 (50.0%)	223.6 (50.0%)
		250	9.2 (50.0%)	9.2 (50.0%)	347.4 (49.7%)	353.0 (50.3%)
	$2\ell+4j$	500	15.2 (48.7%)	16.0 (51.3%)	391.6 (49.3%)	402.5 (50.6%)
		1000	12.5 (49.8%)	12.6 (50.1%)	247.9 (48.7%)	260.6 (51.2%)

Table 18. Number of events containing SSD or OSD and their percentage numbers (in bracket) for different RHN masses (M_N in GeV) with the centre of mass energies of 27, 100 TeV, at the integrated luminosities of 10, 30 ab^{-1} and for $Y_N = 5 \times 10^{-9}$.

situated in one of the hemispheres, it can only tag one RHN leg for a given event. Thus, measurement of OSD:SSD for a given event is not possible inside the MATHUSLA detector and we have to rely on CMS, ATLAS and the proposed FCC-hh detector. Ideally, $pp \to NN \to \ell^\pm\ell^\mp + 2W^\pm$ gives rise to $2\ell+4j$ final state when $W^\pm$ decays hadronically. However, due to the boost effect, the jets coming from the $W^\pm$ can be co-linear making the final state as $2\ell + 2j$ as discussed in the previous section. This occurs mostly when $M_N \lesssim 300\,\text{GeV}$.

It is evident from the previous section, isolation cuts and the boost effect together can alter the ratio of SS:OS from 1:1. This prompt us to reconstruct the RHN legs via the stepwise reconstructions of the $W^\pm$ boson as well as RHN mass M_N. We incorporated advance cuts to ensure that the leptons are coming from opposite legs, i.e. from two different RHNs. This is achieved for $2\ell+4j$ final state by demanding that we observe two $W^\pm$ peaks in a event and then reconstruct two different RHNs by reconstructing the invariant mass $m_{j_i j_j, \ell_k}$, where j_i, j_j corresponds to the two jets coming from the 10 GeV window of the $W^\pm$ peak in the invariant mass distribution of the di-jet, i.e. $m_{j_i j_j}$, and ℓ_k correspond to

JHEP02(2023)103

the hard leptons for two different $m_{j_i j_j, \ell_k}$ distributions. Once the $m_{j_i j_j, \ell_k}$ distributions are formed we demand two peaks around M_N in a given event and demand the leptons to be inside the 10 GeV mass window around $m_{j_i j_j, \ell_k} = M_N$. For $2\ell + 2j$, the Fatjet is formed with the jet mass at $M_{W^\pm}$ and m_{j_i,ℓ_j} peaks around M_N. Charges of these two leptons are then investigated to calculate SSD: OSD as tabulated in table 17 for scenario 1 and table 18 for scenario 2 for both the final states ($2\ell + 2j$ and $2\ell + 4j$). We can remind ourselves that for scenarios 1, as we have considered $U_{\rm PMNS}$, for higher M_N (for $2\ell + 4j$), we do not get any displaced leptons and thus they are not considered here. From table 17 and table 18 we realise that though the Majorana nature (SSD:OSD=1:1) can be restored but the requirements of the additional cuts result in very low number of events and only possible at the HE-LHC and FCC-hh with 27, 100 TeV centre of mass energies at the integrated luminosity of 10, 30 ab^{-1}, respectively. For lower mass values $M_N < M_{W^\pm}$, the $W^\pm$ remains off-shell which makes such reconstruction of RHNs difficult, along with that the lower statistics make it hard to reproduce SSD:OSD=1:1.

7 Discussion and conclusion

In this article, we consider Z_{B-L} model to produce the RHN pairs, which can have displaced decay depending on the Yukawa coupling Y_N. In the scenario-1, we consider Casas-Ibarra parameterization to incorporate the light neutrino mass and mixing angle considering three generations of RHNs. The longitudinal and transverse boost effects are investigated separately and their effects on the displaced decay lengths are extensively studied. In this context the event numbers in CMS, ATLAS and MATHUSLA detectors are shown for HL-LHC and HE-LHC. The event number for the collision with a 100 TeV centre of mass energy is provided for the proposed FCC-hh detector and MATHUSLA as well. Specific final states of 4ℓ, $3\ell+ \geq 1j$, $2\ell+ \geq 2j$ are also studied and we see that BP2, i.e $M_N = 60$ GeV satisfying $U_{\rm PMNS}$ has some promise at the MATHUSLA. The prospect of FASER-II, though not much, but is shown in the displaced decay distributions.

One of the most interesting feature of Majorana fermions, i.e same sign di-lepton (SSD) and opposite sign di-leptons (OSD) come as the same numbers when the leptons directly come from the RHN decay. However, boosted decay products from the RHNs decays are often collinear and fail the jet-lepton isolation criteria and the leptons coming from $W^\pm$ bosons can be misidentified as the leptons coming from RHNs. This results into skewed ratio of SSD:OSD, giving rise to more OSD. A thorough investigation of such effects on RHNs of different masses and for 27, 100 TeV centre mass energies are studied. It has been found that lesser the boost, less skewed is the ratio. A remedy to get back the Majorana signature via successfully tagging the legs are also prescribed. However, such reconstructions of the different RHN legs suffer in the final state event numbers.

For scenario-1 we also have drawn the regions which can be probed at the LHC/FCC with centre of mass energies of 14, 27, 100 TeV at integrated luminosities of 3, 10 and 30 ab^{-1} in the $M_N - M_{Z_{B-L}}$ plane. We see that a lighter mass of RHN i.e. $M_N = 5$ can be probed with a maximum of 900 GeV, whereas Z_{B-L} can be probed up to 15.7 TeV.

In the later part of the article, we consider scenario-2, motivated by the collider searches, where we consider one generation of RHN with small Yukawa coupling, which is

JHEP02(2023)103

a free parameter, while the others can explain the light neutrino masses and mixing. We benchmark the scenario with $M_N = 60, 100\,\text{GeV}$ with $Y_N = 5 \times 10^{-8}$ and 5×10^{-9}. Final states of 4ℓ, $3\ell+ \geq 1j$, $2\ell+ \geq 2j$ are also studied as we found that MATHUSLA regions are preferred by BP2, BP3 for $Y_N = 5 \times 10^{-8}$, 5×10^{-9}, respectively. To complete the study we drew the regions plots in $M_N - M_{Z_{B-L}}$ (in figure 12), $M_{Z_{B-L}} - Y_N$ (in figure 13) and $M_N - Y_N$ (in figure 14) planes, where in figure 13 we assume a hierarchy of $M_{Z_{B-L}} = 10 M_N$. $M_N = 4200\,\text{GeV}$ along with $M_{Z_{B-L}} = 30.5\,\text{TeV}$ can be explored with $Y_N = 5 \times 10^{-9}$ at the FCC-hh with centre of mass energy of 100 TeV. Similarly, Y_N can be probed as low as $\mathcal{O}(10^{-13})$. While considering lighter mass of RHN, $M_N \sim 3\,\text{GeV}$ can also be explored with substantially high values of $Y_N \sim 10^{-3}$.

The study performed in this article can be easily attributed to other U(1)′ models with right-handed neutrino [79–84] and other displaced neutral decays [70, 85, 86]. The segregation of transverse and longitudinal displaced decays manifests the longitudinal boost effect at higher centre of mass energies. Finally general SS:OS signature can be skewed due to the boost effect. However, Majorana nature can be explored via the tagging of the RHNs legs at the CMS, ATLAS and the proposed FCC-hh detector. Due to presence of MATHUSLA detector in one of the hemispheres, it cannot be resolved there and we have to rely on CMS, ATLAS or FCC-hh detector.

Acknowledgments

PB acknowledges SERB CORE Grant CRG/2018/004971 and MATRICS Grant MTR/2020/000668 for the financial and computational support towards the work. PB also acknowledges Anomalies 2019 for the initiation of the project. CS would like to thank MOE Government of India for the SRF. PB and CS would like to express their gratitude to Korea Institute For Advanced Study for arranging a collaborative visit during the last phase of the project.

References

[1] CMS collaboration, *Observation of a new boson at a mass of* 125 *GeV with the CMS experiment at the LHC*, *Phys. Lett. B* **716** (2012) 30 [arXiv:1207.7235] [INSPIRE].

[2] ATLAS collaboration, *Observation of a new particle in the search for the standard model Higgs boson with the ATLAS detector at the LHC*, *Phys. Lett. B* **716** (2012) 1 [arXiv:1207.7214] [INSPIRE].

[3] CMS collaboration, *Measurements of Higgs boson properties in the diphoton decay channel in proton-proton collisions at* $\sqrt{s} = 13$ *TeV*, *JHEP* **11** (2018) 185 [arXiv:1804.02716] [INSPIRE].

JHEP02(2023)103

[4] ATLAS collaboration, *Measurements of Higgs boson properties in the diphoton decay channel with 36 fb^{-1} of pp collision data at $\sqrt{s} = 13$ TeV with the ATLAS detector*, *Phys. Rev. D* **98** (2018) 052005 [arXiv:1802.04146] [INSPIRE].

[5] CMS collaboration, *Measurements of properties of the Higgs boson decaying to a W boson pair in pp collisions at $\sqrt{s} = 13$ TeV*, *Phys. Lett. B* **791** (2019) 96 [arXiv:1806.05246] [INSPIRE].

[6] ATLAS collaboration, *Measurements of gluon-gluon fusion and vector-boson fusion Higgs boson production cross-sections in the $H \to WW^* \to e\nu\mu\nu$ decay channel in pp collisions at $\sqrt{s} = 13$ TeV with the ATLAS detector*, *Phys. Lett. B* **789** (2019) 508 [arXiv:1808.09054] [INSPIRE].

[7] CMS collaboration, *Measurements of properties of the Higgs boson decaying into the four-lepton final state in pp collisions at $\sqrt{s} = 13$ TeV*, *JHEP* **11** (2017) 047 [arXiv:1706.09936] [INSPIRE].

[8] ATLAS collaboration, *Measurements of the Higgs boson inclusive and differential fiducial cross sections in the 4ℓ decay channel at $\sqrt{s} = 13$ TeV*, *Eur. Phys. J. C* **80** (2020) 942 [arXiv:2004.03969] [INSPIRE].

[9] CMS collaboration, *Observation of Higgs boson decay to bottom quarks*, *Phys. Rev. Lett.* **121** (2018) 121801 [arXiv:1808.08242] [INSPIRE].

[10] ATLAS collaboration, *Observation of $H \to b\bar{b}$ decays and VH production with the ATLAS detector*, *Phys. Lett. B* **786** (2018) 59 [arXiv:1808.08238] [INSPIRE].

[11] CMS collaboration, *Observation of the Higgs boson decay to a pair of τ leptons with the CMS detector*, *Phys. Lett. B* **779** (2018) 283 [arXiv:1708.00373] [INSPIRE].

[12] ATLAS collaboration, *Cross-section measurements of the Higgs boson decaying into a pair of τ-leptons in proton-proton collisions at $\sqrt{s} = 13$ TeV with the ATLAS detector*, *Phys. Rev. D* **99** (2019) 072001 [arXiv:1811.08856] [INSPIRE].

[13] S. Okada, *Z' portal dark matter in the minimal B-L model*, *Adv. High Energy Phys.* **2018** (2018) 5340935 [arXiv:1803.06793] [INSPIRE].

[14] L. Basso, A. Belyaev, S. Moretti and C.H. Shepherd-Themistocleous, *Phenomenology of the minimal B-L extension of the standard model: Z' and neutrinos*, *Phys. Rev. D* **80** (2009) 055030 [arXiv:0812.4313] [INSPIRE].

[15] R.N. Mohapatra and R.E. Marshak, *Local B-L symmetry of electroweak interactions, Majorana neutrinos and neutron oscillations*, *Phys. Rev. Lett.* **44** (1980) 1316 [*Erratum ibid.* **44** (1980) 1643] [INSPIRE].

[16] P. Bandyopadhyay, E.J. Chun and R. Mandal, *Implications of right-handed neutrinos in B-L extended standard model with scalar dark matter*, *Phys. Rev. D* **97** (2018) 015001 [arXiv:1707.00874] [INSPIRE].

[17] F. Deppisch, S. Kulkarni and W. Liu, *Heavy neutrino production via Z' at the lifetime frontier*, *Phys. Rev. D* **100** (2019) 035005 [arXiv:1905.11889] [INSPIRE].

[18] C.-W. Chiang, G. Cottin, A. Das and S. Mandal, *Displaced heavy neutrinos from Z' decays at the LHC*, *JHEP* **12** (2019) 070 [arXiv:1908.09838] [INSPIRE].

[19] W. Liu, S. Kulkarni and F.F. Deppisch, *Heavy neutrinos at the FCC-hh in the $\mathrm{U}(1)_{B-L}$ model*, *Phys. Rev. D* **105** (2022) 095043 [arXiv:2202.07310] [INSPIRE].

JHEP02(2023)103

[20] A. Das, S. Mandal, T. Nomura and S. Shil, *Heavy Majorana neutrino pair production from Z' at hadron and lepton colliders*, *Phys. Rev. D* **105** (2022) 095031 [arXiv:2202.13358] [INSPIRE].

[21] R. Padhan, M. Mitra, S. Kulkarni and F.F. Deppisch, *Displaced fat-jets and tracks to probe boosted right-handed neutrinos in the $\mathrm{U}(1)_{B-L}$ model*, *Eur. Phys. J. C* **82** (2022) 858 [arXiv:2203.06114] [INSPIRE].

[22] P. Fileviez Perez, T. Han and T. Li, *Testability of type I seesaw at the CERN LHC: revealing the existence of the $B-L$ symmetry*, *Phys. Rev. D* **80** (2009) 073015 [arXiv:0907.4186] [INSPIRE].

[23] Z. Kang, P. Ko and J. Li, *New avenues to heavy right-handed neutrinos with pair production at hadronic colliders*, *Phys. Rev. D* **93** (2016) 075037 [arXiv:1512.08373] [INSPIRE].

[24] A. Das and N. Okada, *Bounds on heavy Majorana neutrinos in type-I seesaw and implications for collider searches*, *Phys. Lett. B* **774** (2017) 32 [arXiv:1702.04668] [INSPIRE].

[25] T. Han and B. Zhang, *Signatures for Majorana neutrinos at hadron colliders*, *Phys. Rev. Lett.* **97** (2006) 171804 [hep-ph/0604064] [INSPIRE].

[26] P.S.B. Dev, A. Pilaftsis and U.-K. Yang, *New production mechanism for heavy neutrinos at the LHC*, *Phys. Rev. Lett.* **112** (2014) 081801 [arXiv:1308.2209] [INSPIRE].

[27] E. Accomando, L. Delle Rose, S. Moretti, E. Olaiya and C.H. Shepherd-Themistocleous, *Extra Higgs boson and Z' as portals to signatures of heavy neutrinos at the LHC*, *JHEP* **02** (2018) 109 [arXiv:1708.03650] [INSPIRE].

[28] P. Bandyopadhyay, M. Mitra and A. Roy, *Relativistic freeze-in with scalar dark matter in a gauged B-L model and electroweak symmetry breaking*, *JHEP* **05** (2021) 150 [arXiv:2012.07142] [INSPIRE].

[29] W. Rodejohann and C.E. Yaguna, *Scalar dark matter in the B-L model*, *JCAP* **12** (2015) 032 [arXiv:1509.04036] [INSPIRE].

[30] P. Bandyopadhyay, M. Mitra, R. Padhan, A. Roy and M. Spannowsky, *Secluded dark matter in gauged B-L model*, *JHEP* **05** (2022) 182 [arXiv:2201.09203] [INSPIRE].

[31] E. Izaguirre and B. Shuve, *Multilepton and lepton jet probes of sub-weak-scale right-handed neutrinos*, *Phys. Rev. D* **91** (2015) 093010 [arXiv:1504.02470] [INSPIRE].

[32] I. Zurbano Fernandez et al., *High-Luminosity Large Hadron Collider (HL-LHC): technical design report*, Tech. Rep. CERN-2020-010, CERN, Geneva, Switzerland (2020) [INSPIRE].

[33] FCC collaboration, *HE-LHC: the High-Energy Large Hadron Collider. Future Circular Collider conceptual design report volume* 4, *Eur. Phys. J. ST* **228** (2019) 1109 [INSPIRE].

[34] FCC collaboration, *FCC-hh: the hadron collider. Future Circular Collider conceptual design report volume* 3, *Eur. Phys. J. ST* **228** (2019) 755 [INSPIRE].

[35] S. Khalil, *TeV-scale gauged B-L symmetry with inverse seesaw mechanism*, *Phys. Rev. D* **82** (2010) 077702 [arXiv:1004.0013] [INSPIRE].

[36] P. Bandyopadhyay, E.J. Chun, H. Okada and J.-C. Park, *Higgs signatures in inverse seesaw model at the LHC*, *JHEP* **01** (2013) 079 [arXiv:1209.4803] [INSPIRE].

[37] J.A. Casas and A. Ibarra, *Oscillating neutrinos and $\mu \to e, \gamma$*, *Nucl. Phys. B* **618** (2001) 171 [hep-ph/0103065] [INSPIRE].

JHEP02(2023)103

[38] Particle Data Group collaboration, *Review of particle physics*, *PTEP* **2020** (2020) 083C01 [INSPIRE].

[39] F.F. Deppisch, W. Liu and M. Mitra, *Long-lived heavy neutrinos from Higgs decays*, *JHEP* **08** (2018) 181 [arXiv:1804.04075] [INSPIRE].

[40] W. Liu, J. Li, J. Li and H. Sun, *Testing the seesaw mechanisms via displaced right-handed neutrinos from a light scalar at the HL-LHC*, *Phys. Rev. D* **106** (2022) 015019 [arXiv:2204.03819] [INSPIRE].

[41] W. Abdallah, A. Awad, S. Khalil and H. Okada, *Muon anomalous magnetic moment and $\mu \to e\gamma$ in B-L model with inverse seesaw*, *Eur. Phys. J. C* **72** (2012) 2108 [arXiv:1105.1047] [INSPIRE].

[42] M. Carena, A. Daleo, B.A. Dobrescu and T.M.P. Tait, *Z' gauge bosons at the Tevatron*, *Phys. Rev. D* **70** (2004) 093009 [hep-ph/0408098] [INSPIRE].

[43] ATLAS collaboration, *Search for high-mass dilepton resonances using 139 fb^{-1} of pp collision data collected at $\sqrt{s} = 13$ TeV with the ATLAS detector*, *Phys. Lett. B* **796** (2019) 68 [arXiv:1903.06248] [INSPIRE].

[44] CMS collaboration, *Search for resonant and nonresonant new phenomena in high-mass dilepton final states at $\sqrt{s} = 13$ TeV*, *JHEP* **07** (2021) 208 [arXiv:2103.02708] [INSPIRE].

[45] W. Liao and X.-H. Wu, *Signature of heavy sterile neutrinos at CEPC*, *Phys. Rev. D* **97** (2018) 055005 [arXiv:1710.09266] [INSPIRE].

[46] M. Klasen, F. Lyonnet and F.S. Queiroz, *NLO+NLL collider bounds, Dirac fermion and scalar dark matter in the B-L model*, *Eur. Phys. J. C* **77** (2017) 348 [arXiv:1607.06468] [INSPIRE].

[47] F. Staub, *SARAH 4: a tool for (not only SUSY) model builders*, *Comput. Phys. Commun.* **185** (2014) 1773 [arXiv:1309.7223] [INSPIRE].

[48] A. Belyaev, N.D. Christensen and A. Pukhov, *CalcHEP 3.4 for collider physics within and beyond the standard model*, *Comput. Phys. Commun.* **184** (2013) 1729 [arXiv:1207.6082] [INSPIRE].

[49] NNPDF collaboration, *A first unbiased global determination of polarized PDFs and their uncertainties*, *Nucl. Phys. B* **887** (2014) 276 [arXiv:1406.5539] [INSPIRE].

[50] M. Aleksa et al., *Calorimeters for the FCC-hh*, Tech. Rep. CERN-FCC-PHYS-2019-0003 (2019) [arXiv:1912.09962] [INSPIRE].

[51] W. Riegler, *FCC-hh detector: FCC CDR summary report, status of detailed report*, in FCC week, Brussels, Belgium, 26 June 2019.

[52] D. Curtin et al., *Long-lived particles at the energy frontier: the MATHUSLA physics case*, *Rept. Prog. Phys.* **82** (2019) 116201 [arXiv:1806.07396] [INSPIRE].

[53] T. Sjöstrand et al., *An introduction to PYTHIA 8.2*, *Comput. Phys. Commun.* **191** (2015) 159 [arXiv:1410.3012] [INSPIRE].

[54] M. Cacciari, G.P. Salam and G. Soyez, *FastJet user manual*, *Eur. Phys. J. C* **72** (2012) 1896 [arXiv:1111.6097] [INSPIRE].

[55] P. Bandyopadhyay and B. Bhattacherjee, *Boosted top quarks in supersymmetric cascade decays at the LHC*, *Phys. Rev. D* **84** (2011) 035020 [arXiv:1012.5289] [INSPIRE].

JHEP02(2023)103

[56] A. Bhardwaj, A. Das, P. Konar and A. Thalapillil, *Looking for minimal inverse seesaw scenarios at the LHC with jet substructure techniques*, *J. Phys. G* **47** (2020) 075002 [arXiv:1801.00797] [INSPIRE].

[57] S. Chakraborty, M. Mitra and S. Shil, *Fat jet signature of a heavy neutrino at lepton collider*, *Phys. Rev. D* **100** (2019) 015012 [arXiv:1810.08970] [INSPIRE].

[58] S. Ashanujjaman, D. Choudhury and K. Ghosh, *Search for exotic leptons in final states with two or three leptons and fat-jets at* 13 *TeV LHC*, *JHEP* **04** (2022) 150 [arXiv:2201.09645] [INSPIRE].

[59] S. Ashanujjaman and K. Ghosh, *Type-III see-saw: search for triplet fermions in final states with multiple leptons and fat-jets at* 13 *TeV LHC*, *Phys. Lett. B* **825** (2022) 136889 [arXiv:2111.07949] [INSPIRE].

[60] C. Bierlich et al., *A comprehensive guide to the physics and usage of PYTHIA* 8.3, Tech. Rep. LU-TP 22-16 (2022) [*SciPost Phys. Codebases* **8** (2022)] [arXiv:2203.11601] [INSPIRE].

[61] CMS collaboration, *Search for long-lived particles decaying to leptons with large impact parameter in proton-proton collisions at* $\sqrt{s} = 13$ *TeV*, *Eur. Phys. J. C* **82** (2022) 153 [arXiv:2110.04809] [INSPIRE].

[62] ATLAS collaboration, *Search for displaced leptons in* $\sqrt{s} = 13$ *TeV pp collisions with the ATLAS detector*, *Phys. Rev. Lett.* **127** (2021) 051802 [arXiv:2011.07812] [INSPIRE].

[63] CMS collaboration, *CMS technical design report, volume II: physics performance*, *J. Phys. G* **34** (2007) 995 [INSPIRE].

[64] ATLAS collaboration, *ATLAS detector and physics performance: technical design report,* 1, Tech. Rep. CERN-LHCC-99-014, CERN, Geneva, Switzerland (1999).

[65] MATHUSLA collaboration, *Explore the lifetime frontier with MATHUSLA*, 2020 *JINST* **15** C06026 [arXiv:1901.04040] [INSPIRE].

[66] J.P. Chou, D. Curtin and H.J. Lubatti, *New detectors to explore the lifetime frontier*, *Phys. Lett. B* **767** (2017) 29 [arXiv:1606.06298] [INSPIRE].

[67] A. Coccaro, D. Curtin, H.J. Lubatti, H. Russell and J. Shelton, *Data-driven model-independent searches for long-lived particles at the LHC*, *Phys. Rev. D* **94** (2016) 113003 [arXiv:1605.02742] [INSPIRE].

[68] C. Alpigiani, *Exploring the lifetime and cosmic frontier with the MATHUSLA detector*, 2020 *JINST* **15** C09048 [arXiv:2006.00788] [INSPIRE].

[69] D. Cartin, private communication.

[70] B. Bhattacherjee, S. Matsumoto and R. Sengupta, *Long-lived light mediators from Higgs boson decay at HL-LHC and FCC-hh, and a proposal of dedicated long-lived particle detectors for FCC-hh*, *Phys. Rev. D* **106** (2022) 095018 [arXiv:2111.02437] [INSPIRE].

[71] FASER collaboration, *FASER: ForwArd Search ExpeRiment at the LHC*, Tech. Rep. UCI-TR-2019-01 (2019) [arXiv:1901.04468] [INSPIRE].

[72] FASER collaboration, *FASER's physics reach for long-lived particles*, *Phys. Rev. D* **99** (2019) 095011 [arXiv:1811.12522] [INSPIRE].

[73] Particle Data Group collaboration, *Review of particle physics*, *PTEP* **2020** (2020) 083C01 [INSPIRE].

JHEP02(2023)103

[74] G. Cowan, *Statistics* (40), https://pdg.lbl.gov/2017/reviews/rpp2017-rev-statistics.pdf, September 2017.

[75] C. Sen, P. Bandyopadhyay, S. Dutta and A. KT, *Displaced Higgs production in type-III seesaw at the LHC/FCC, MATHUSLA and muon collider*, *Eur. Phys. J. C* **82** (2022) 230 [arXiv:2107.12442] [INSPIRE].

[76] C.-Y. Chen and P.S.B. Dev, *Multi-lepton collider signatures of heavy Dirac and Majorana neutrinos*, *Phys. Rev. D* **85** (2012) 093018 [arXiv:1112.6419] [INSPIRE].

[77] CMS collaboration, *Search for heavy Majorana neutrinos in same-sign dilepton channels in proton-proton collisions at* $\sqrt{s} = 13$ *TeV*, *JHEP* **01** (2019) 122 [arXiv:1806.10905] [INSPIRE].

[78] A. Das, P.S.B. Dev and R.N. Mohapatra, *Same sign versus opposite sign dileptons as a probe of low scale seesaw mechanisms*, *Phys. Rev. D* **97** (2018) 015018 [arXiv:1709.06553] [INSPIRE].

[79] P. Bandyopadhyay, E.J. Chun and J.-C. Park, *Right-handed sneutrino dark matter in* U(1)′ *seesaw models and its signatures at the LHC*, *JHEP* **06** (2011) 129 [arXiv:1105.1652] [INSPIRE].

[80] P. Bandyopadhyay, *Displaced lepton flavour violating signatures of right-handed sneutrinos in* U(1)′ *supersymmetric models*, *JHEP* **09** (2017) 052 [arXiv:1511.03842] [INSPIRE].

[81] P. Bandyopadhyay and E.J. Chun, *Lepton flavour violating signature in supersymmetric* U(1)′ *seesaw models at the LHC*, *JHEP* **05** (2015) 045 [arXiv:1412.7312] [INSPIRE].

[82] P. Bandyopadhyay, E.J. Chun and R. Mandal, *Implications of right-handed neutrinos in B-L extended standard model with scalar dark matter*, *Phys. Rev. D* **97** (2018) 015001 [arXiv:1707.00874] [INSPIRE].

[83] E. Accomando, L. Delle Rose, S. Moretti, E. Olaiya and C.H. Shepherd-Themistocleous, *Novel SM-like Higgs decay into displaced heavy neutrino pairs in* U(1)′ *models*, *JHEP* **04** (2017) 081 [arXiv:1612.05977] [INSPIRE].

[84] E. Accomando, C. Coriano, L. Delle Rose, J. Fiaschi, C. Marzo and S. Moretti, *Z′, Higgses and heavy neutrinos in* U(1)′ *models: from the LHC to the GUT scale*, *JHEP* **07** (2016) 086 [arXiv:1605.02910] [INSPIRE].

[85] A. Sabancı Keceli, P. Bandyopadhyay and K. Huitu, *Long-lived triplinos and displaced lepton signals at the LHC*, *Eur. Phys. J. C* **79** (2019) 345 [arXiv:1810.09172] [INSPIRE].

[86] P. Bandyopadhyay, P. Ghosh and S. Roy, *Unusual Higgs boson signal in R-parity violating nonminimal supersymmetric models at the LHC*, *Phys. Rev. D* **84** (2011) 115022 [arXiv:1012.5762] [INSPIRE].

JHEP02(2023)103